

RECORD  
2023/5

# SPATIAL TRENDS AND RELATIONSHIPS EMERGING FROM THE SYSTEMATIC CLASSIFICATION OF GRANITIC ROCKS OF THE YILGARN CRATON

RH Smithies, JR Lowrey, DC Champion, Y Lu and K Gessner



Government of Western Australia  
Department of Mines, Industry Regulation and Safety

Geological Survey of  
Western Australia





Government of **Western Australia**  
Department of **Mines, Industry Regulation  
and Safety**

RECORD 2023/5

# SPATIAL TRENDS AND RELATIONSHIPS EMERGING FROM THE SYSTEMATIC CLASSIFICATION OF GRANITIC ROCKS OF THE YILGARN CRATON

RH Smithies, JR Lowrey, DC Champion\*, Y Lu and K Gessner

\* Geoscience Australia, GPO Box 378, Canberra ACT 2601

PERTH 2023



**Geological Survey of  
Western Australia**



**MINISTER FOR MINES AND PETROLEUM**  
**Hon Bill Johnston MLA**

**DIRECTOR GENERAL, DEPARTMENT OF MINES, INDUSTRY REGULATION AND SAFETY**  
**Richard Sellers**

**EXECUTIVE DIRECTOR, GEOLOGICAL SURVEY AND RESOURCE STRATEGY**  
**Michele Spencer**

#### **REFERENCE**

**The recommended reference for this publication is:**

Smithies, RH, Lowrey, JR, Champion, DC, Lu, Y and Gessner, K 2023, Spatial trends and relationships emerging from the systematic classification of granitic rocks of the Yilgarn Craton: Geological Survey of Western Australia, Record 2023/5, 33p.

**ISBN** 978-1-74168-005-8

**ISSN** 2204-4345

Grid references in this publication refer to the Geocentric Datum of Australia 1994 (GDA94). Locations mentioned in the text are referenced using Map Grid Australia (MGA) coordinates, Zone 50. All locations are quoted to at least the nearest 100 m.



Australian Government  
Geoscience Australia

#### **Disclaimer**

This product uses information from various sources. The Department of Mines, Industry Regulation and Safety (DMIRS) and the State cannot guarantee the accuracy, currency or completeness of the information. Neither the department nor the State of Western Australia nor any employee or agent of the department shall be responsible or liable for any loss, damage or injury arising from the use of or reliance on any information, data or advice (including incomplete, out of date, incorrect, inaccurate or misleading information, data or advice) expressed or implied in, or coming from, this publication or incorporated into it by reference, by any person whosoever.

#### **Published 2023 by the Geological Survey of Western Australia**

This Record is published in digital format (PDF) and is available online at <[www.dmirs.wa.gov.au/GSWApublications](http://www.dmirs.wa.gov.au/GSWApublications)>.



© State of Western Australia (Department of Mines, Industry Regulation and Safety) 2023

With the exception of the Western Australian Coat of Arms and other logos, and where otherwise noted, these data are provided under a Creative Commons Attribution 4.0 International Licence. (<https://creativecommons.org/licenses/by/4.0/legalcode>)

#### **Further details of geoscience products are available from:**

First Floor Counter  
Department of Mines, Industry Regulation and Safety  
100 Plain Street  
EAST PERTH WESTERN AUSTRALIA 6004  
Telephone: +61 8 9222 3459 Email: [publications@dmirs.wa.gov.au](mailto:publications@dmirs.wa.gov.au)  
[www.dmirs.wa.gov.au/GSWApublications](http://www.dmirs.wa.gov.au/GSWApublications)

**Cover image:** Episodic tides discharge sediments along a rocky shoreline at Cable Beach, Broome. Photo by Robin Bower

# Contents

Summary .....	1
Introduction .....	1
A note on granite classification .....	4
Broad geographical and temporal distribution of granite types .....	4
High-Ca (low-Sr/Y) granites .....	4
High-Ca (high-Sr/Y) granites .....	5
Low-Ca granites .....	11
Low-Ca (high-Ti) granites .....	11
High field strength element granites .....	18
Syenites .....	18
Sanukitoids .....	18
Spatial relationships and trends between sanukitoids and syenites .....	20
Sanukitoid-like rocks .....	21
Diorite .....	23
Significance of regional- and craton-scale trends .....	25
Regional granite domains .....	25
Young juvenile crustal additions .....	28
Other patterns .....	30
Granites, greenstones and gold .....	30
Conclusions .....	32
References .....	32

## Appendix

*Available with the PDF online as an accompanying digital resource*

1. Layered PDF version of Figure 2

## Figures

1. Distribution of felsic rock samples in the Yilgarn Craton .....	2
2. Distribution of the fully classified granite dataset .....	3
3. Zircon igneous crystallization age distribution for samples .....	5
4. Distribution of High-Ca, low-Sr/Y granites .....	6
5. Distribution of High-Ca, low-Sr/Y granites vs regional isotopic data .....	7
6. Distribution of samples with zircon igneous crystallization ages .....	8
7. Distribution of all High-Ca granites .....	9
8. Distribution of a) High-Ca (Na+), high-Sr/Y granites; b) all High-Ca, high-Sr/Y granites .....	10
9. Distribution of all Low-Ca granites .....	12
10. Zircon saturation temperatures for a) all samples; b) Low-Ca granites and Low-Ca (high-Ti) granites .....	13
11. Distribution of Low-Ca granites with zircon saturation temperatures >820 °C .....	14
12. Distribution model ages ( $T_{DM}^2$ ) (Nd-isotope) .....	15
13. Distribution of Low-Ca granites and Low-Ca (high-Ti) granites vs regional isotopic data .....	16
14. Regional $\epsilon_{Nd}$ data .....	17
15. Distribution of high-HFSE granites and potential linear trends .....	19
16. AFM diagram showing various granite classes .....	20
17. Zircon igneous crystallization age ranges for various granites .....	20
18. TAS diagram for syenites and sanukitoids .....	21
19. Distribution of: a) syenites; b) sanukitoids .....	22
20. Distribution and regional trends of syenites, sanukitoids and high-HFSE granites .....	23
21. Distribution of sanukitoid, sanukitoid-like rocks and diorite .....	24
22. Regional granite data with symbol size scaled to Sr/Y ratio .....	26
23. Distribution of High-Ca, high-Sr/Y granites, sanukitoids and syenites vs regional isotopic data .....	27
24. Comparison of regional Nd-isotope maps contoured using a range of lithologies .....	29
25. Distribution of sanukitoids and syenites and gold deposits vs regional isotopic data .....	31



# Spatial trends and relationships emerging from the systematic classification of granitic rocks of the Yilgarn Craton

RH Smithies, JR Lowrey, DC Champion\*, Y Lu and K Gessner

## Summary

The Geological Survey of Western Australia (GSWA) has reanalysed an extensive archive of felsic rock samples collected primarily by Geoscience Australia during several regional research programs in the 1990s and 2000s. To ensure an internally consistent dataset, high-quality whole rock major and trace element data were collected using a single suite of analytical techniques at a single analytical laboratory. Using these, and other recently collected high-quality data, approximately 6000 felsic rocks were classified using a purely geochemical classification scheme designed to replicate the granite classification scheme that Champion and Sheraton (1997) constructed for Yilgarn granites, itself a geochemical scheme based on extensive consideration of field relationships and petrographic studies. The resulting spatial patterns within and between specific classified groups highlights local to craton-wide trends that are interpreted to reflect variations in bulk source compositions, lithosphere-scale architecture and melting conditions. An early (pre-3000 Ma) refractory source component is inferred in the crustal source region of some granites (mainly Low-Ca granites) in the Youanmi Terrane. Easterly, or northeasterly, trending regions of high-Sr/Y, and generally sodic, granites in the northern and southern regions of the craton possibly also reflect compositionally distinctive crustal source regions. In the eastern Yilgarn Craton, the distribution of granites that include a significant direct mantle source component is constrained by major northwest-striking structures and by proximity to northwest-striking greenstone belts and in the case of sanukitoids, strongly correlates with the occurrence of gold mineralization.

**KEYWORDS:** Archean, crustal evolution, geochemistry, granitic rocks, Yilgarn Craton

## Introduction

We have systematically applied a consistent geochemical classification scheme (Lowrey et al., 2023) to a large dataset of analyses of felsic rocks from the Archean Yilgarn Craton mainly consisting of recently acquired high-quality data obtained through consistent analytical techniques at a single laboratory (Lowrey et al., 2022). The aim is to present updated and new datasets and classification tools applicable to felsic rocks that might enhance our general understanding of the Archean evolution of the craton and its various mineral systems. This study builds on a considerable body of previous work, primarily by Geoscience Australia (GA), on the petrogenesis, distribution and classification of Yilgarn Craton granites, and on their geodynamic implications (e.g. Champion and Sheraton, 1997; Champion and Cassidy, 2002).

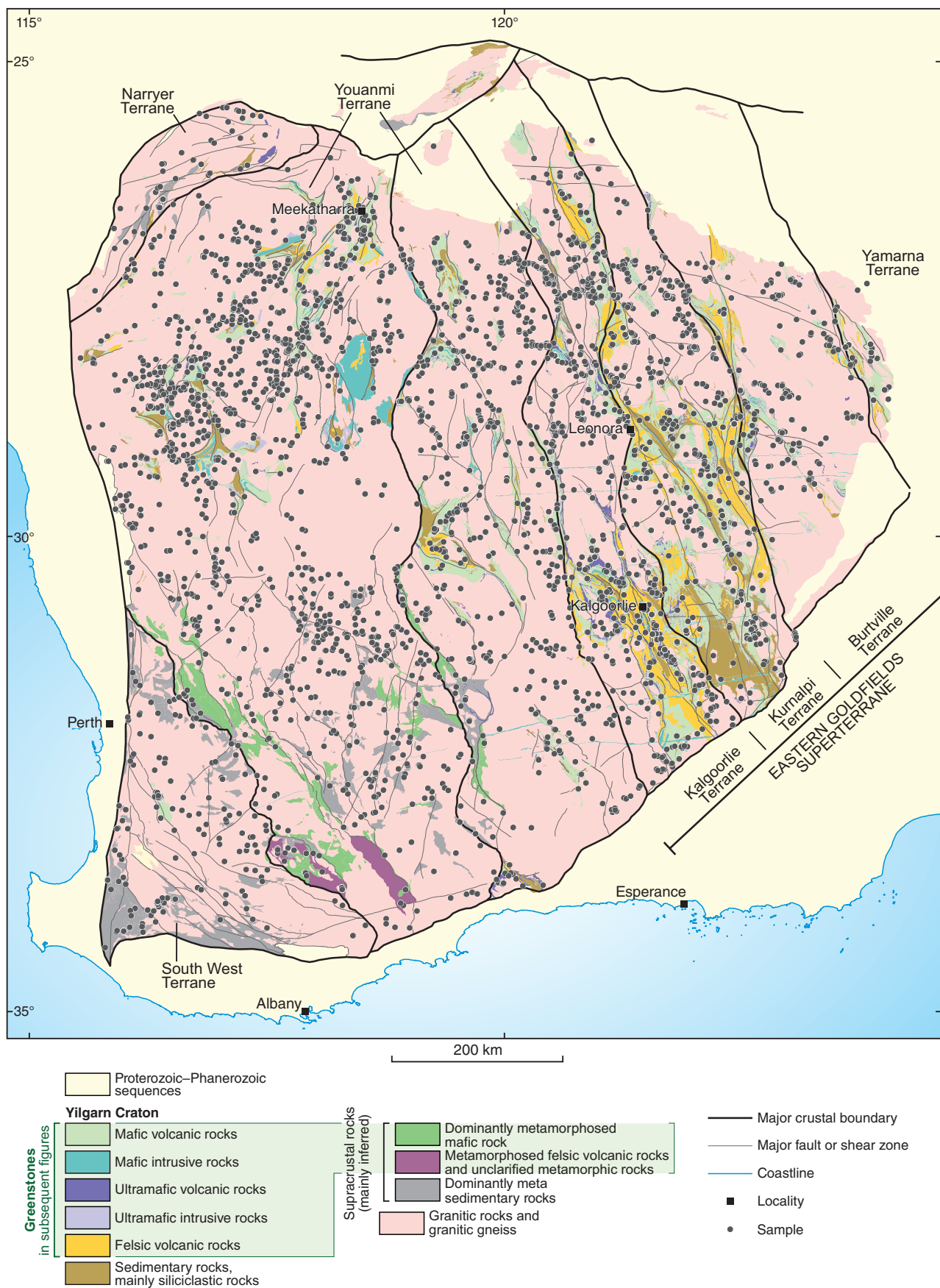
Granitic rocks of the Yilgarn Craton have traditionally been divided based on the classification scheme of Champion and Sheraton (1997), modified by Champion and Cassidy (2002). Lowrey et al. (2023) placed a series of clear compositional boundaries on the various granite compositional groups and provided a workflow that systematically allows each group to be isolated. Lowrey et al. (2023) also expanded this classification by adding additional proxies reflecting variations in source compositions and melting conditions.

Geochemical data presented in Lowrey et al. (2022) include approximately 3000 high-quality whole rock major and trace element analyses, the majority being on GA legacy material reanalysed under the collaborative Geological Survey of Western Australia (GSWA) and GA Yilgarn Granite Geochemistry project. To this dataset, we have added felsic granitic (mainly subvolcanic) and volcanic data collected as part of GSWA's Greenstone geochemical barcoding project (Lowrey and Smithies, 2022). We have also added a range of older analyses of granitic rocks from GSWA and GA archive collections (all soon to be reanalysed as part of the Yilgarn Granite Geochemistry project) and from literature sources. All data, including those from volcanic rocks, have been classified following the procedure set out in Lowrey et al. (2023) for intrusive felsic rocks of the Yilgarn Craton. Smithies et al. (2019) noted that the felsic volcanic and proximal volcanoclastic rocks of the Black Flag Group (Kalgoorlie Terrane) shared the same igneous geochemical trends as the co-magmatic subvolcanic intrusions – justifying inclusion within this study. The final dataset includes approximately 5990 analyses and covers the vast majority of the exposed Yilgarn Craton (Figs 1, 2).

Sample density throughout the craton is variable. There is some inherent bias in this sample set, resulting in gaps in areas of large or abundant salt lakes and laterite cover. However, the distribution and density of samples is extremely good for an Archean craton.

---

\* Geoscience Australia, GPO Box 378, Canberra ACT 2601

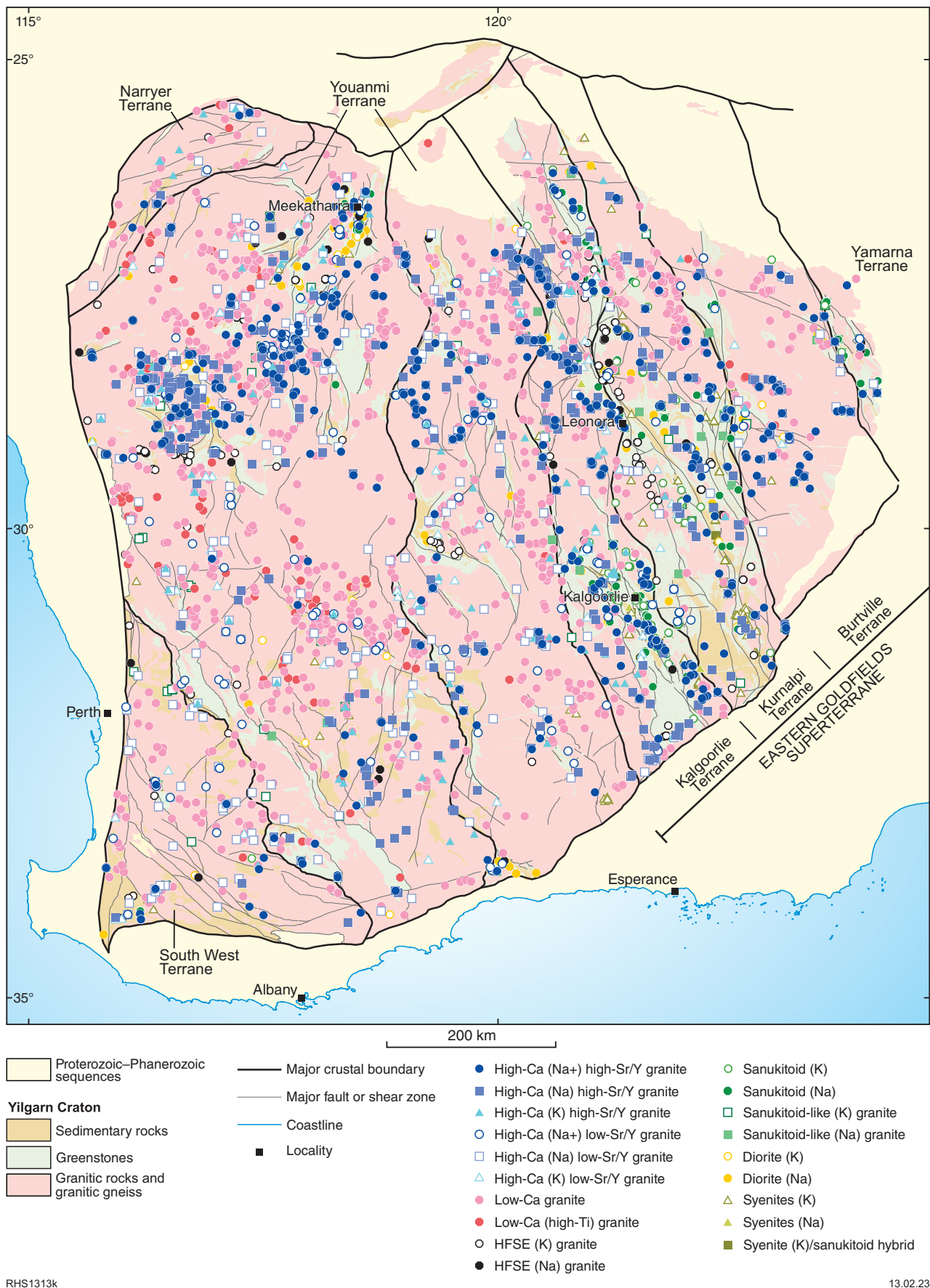


RHS1313p

04.04.23

Figure 1. Summarized bedrock geology of the Yilgarn Craton showing the distribution of felsic rock samples considered here. Terranes after Cassidy et al. (2006), Pawley et al. (2012) and Quentin de Gromard et al. (2021)





RHS1313k

13.02.23

Figure 2. Summarized bedrock geology of the Yilgarn Craton showing the fully classified dataset. Note that where several samples are from a single locality, only the 'top' symbol is visible. Appendix 1 (online version) includes a layered pdf that permits the user to select the granite classifications that are displayed

Areas of lower sample density include the central, southwest and far northwest Youanmi Terrane, the Narryer and South West Terranes and in the eastern parts of the Eastern Goldfields Superterrane (EGST). A high sample density occurs in the northwest Youanmi Terrane and in large parts of the southern and eastern EGST (Fig. 1).

An existing, extensive, geochronological database (~450 age determinations; Geological Survey of Western Australia, 2022) covering felsic rocks of the Yilgarn Craton allows for limited assessment of compositional variations with time, although our conclusions in this regards differ little from those of Czarnota et al. (2010).

The new granite geochemical dataset provides an opportunity to investigate, temporally and spatially, compositional variations in granitic rocks and crustal granite sources, as well as melting conditions and modes of granite emplacement. The observed or inferred spatial and temporal relationships, at various scales, permit broad inferences regarding lithospheric compositional and architectural evolution of the Yilgarn Craton at its mineral systems.

## A note on granite classification

In the process of devising a compositional scheme for separating the various granitic compositional groups, an appreciation was immediately gained of the continuous nature of the bulk of the granite compositional data. This emphasizes a large degree of overlap in the range and influence of magma-forming processes and source compositions in Archean and younger granitic rocks. Examples representing one specific tectonomagmatic process or a single 'pure' source are a minority; in their geochemistry, the great majority of samples show the effects of a range of competing processes, and the petrogenetic ambiguities associated with this are a frustrating reality of studies of granite. The result is that some of the compositional boundaries used in the classification scheme are partly arbitrary, although natural low points in data density distribution are exploited where possible. Other boundaries, for example the  $Mg^\#$ , Cr and Ni ranges defining sanukitoids (Shirey and Hanson, 1984; Stern et al., 1989; Martin et al., 2005) or Sr/Y and  $K_2O/Na_2O$  ranges expected of tonalite–trondjemite–granodiorite series granitic rocks (encompassed within the High-Ca granite group of Champion and Sheraton, 1997) (Martin et al., 2005; Moyen and Martin, 2012; Smithies et al., 2018a), reflect previously defined compositional fields. However, many of the broader compositional boundaries and fields are based on comparisons with compositional fields in the earlier-classified data from Champion and Sheraton (1997) and Champion and Cassidy (2002), in which additional emphasis was placed on textural and mineralogical data. Users of this classification scheme must remain cognizant of these limitations, and specifically, of the use of geochemical data alone to place specific names on rocks that have evolved within complex geological systems. Ultimately, it is the user's responsibility to assess results, particularly unexpected results, within the context of other available geological data; for example, a single sample classified as a syenite within a sea of Low-Ca granites, deserves further scrutiny.

Champion and Sheraton's High-Ca granite group was interpreted to reflect partial melting of a hydrated mafic

crustal source. We further split this between high- and low-Sr/Y subdivisions interpreted to reflect enriched and/or deep (i.e. >40 km) sources (Sr/Y >40) or unenriched and/or shallow sources (Sr/Y <40 km). High-Ca granites (both high- and low-Sr/Y) were also split into 'very sodic' (Na+), 'sodic' (Na) and 'potassic' (K) subgroups based on  $K_2O/Na_2O$  ranges of 0 – 0.6, >0.6 – 1.0 and >1.0 respectively, interpreted to reflect varying amounts of reworked crustal material contributing K to otherwise K-poor 'basaltic' bulk source compositions and/or reflecting decreasing degrees of partial melting.

Low-Ca granite – ranging to higher  $SiO_2$ ,  $K_2O$ , and incompatible trace element concentrations than most High-Ca granites – are interpreted to reflect re-melting of a bulk source that was on average more evolved (i.e. reworked High-Ca granite ± mafic crust ± sedimentary rocks; Champion and Sheraton, 1997) and drier than the source for High-Ca granites, and typically at higher temperatures. We have identified a subclass of Low-Ca granites with high  $TiO_2$  and  $P_2O_5$  contents, locally including orthopyroxene-bearing examples (i.e. charnockites), which reflects additionally high-temperature (>800 °C) crustal melting of a dry and refractory source. Lowrey et al. (2023) refers to these as 'Low-Ca (high-Ti) granites'.

Champion and Sheraton's 'mafic granite' group was subdivided based on proxies for degree of source evolution [ $Mg^\#$  = molecular ratio of  $MgO/(MgO + FeO)$  with total Fe calculated as  $Fe^{2+}$ ] and source enrichment. Thus, this group was divided into:

- Sanukitoids: high  $Mg^\#$  ( $Mg^\# >50$  at 60 wt%  $SiO_2$ ), high Cr and Ni (at 60 wt%  $SiO_2$ , Cr >80 ppm, Ni >50 ppm) high Sr/Y >30. Note that this definition is considerably less restrictive than the original definition for sanukitoid and is based on the observation that many discrete mafic granite bodies containing a large number of samples meeting the strict definition (at 60 wt%  $SiO_2$   $Mg^\# >60$ , Cr and Ni >100 ppm; Shirey and Hanson, 1984; Stern et al., 1989) also show a range to these lower values.
- Sanukitoid-like rocks: lower  $Mg^\#$  ( $Mg^\# 35–50$  at 60 wt%  $SiO_2$ ), low Cr and Ni (at 60 wt%  $SiO_2$ , Cr <80 ppm, Ni <50 ppm) high Sr/Y >30.
- Diorites: Sr/Y <30.

Syenites, high field strength element (HFSE) granites as well as all groups previously encompassed under the mafic granite classification were also divided into K-rich and Na-rich based on a  $K_2O/Na_2O$  boundary of 0.6.

## Broad geographical and temporal distribution of granite types

### High-Ca (low-Sr/Y) granites

This classification of granite is dominated by the sodic (Na) subgroup (52%). There is a weak trend towards K-rich compositions with decreasing age, although the potassic (K) subgroup represents <20% of all High-Ca (low-Sr/Y) granites. All examples with ages >2700 Ma are either Na or Na+ varieties, although the main period of intrusion for



all subgroups was between 2680 and 2720 Ma (Fig. 3a). Older examples are found in all terranes, but only the Narryer Terrane includes ages >3000 Ma.

High-Ca (low-Sr/Y) granites form a major component of the major expanses of granitic rocks away from greenstone belts – less commonly forming intrusions within greenstone belts (Fig. 4). In some regions, and in particular in the northern Youanmi Terrane, these granites appear to be spatially associated with mapped shear zones. Also in this region, Na<sup>+</sup> High-Ca (low-Sr/Y) granites form a north-northeast trend axial to a broader zone characterized by distinctly radiogenic crust and correspondingly young  $T_{DM}^2$  ages (<3.0 Ga) on Nd- and Hf-isotope maps (Fig. 5). This zone is herein informally referred to as the Cue isotopic zone. Na and K High-Ca subgroups are also widely distributed across the craton but are significantly less common within the central region of the Youanmi Terrane, which reflects a region of particularly poor outcrop. The Na and K High-Ca (low-Sr/Y) subgroups are also widely scattered within the Cue isotopic zone, perhaps more commonly at the margins of this zone (Fig. 5).

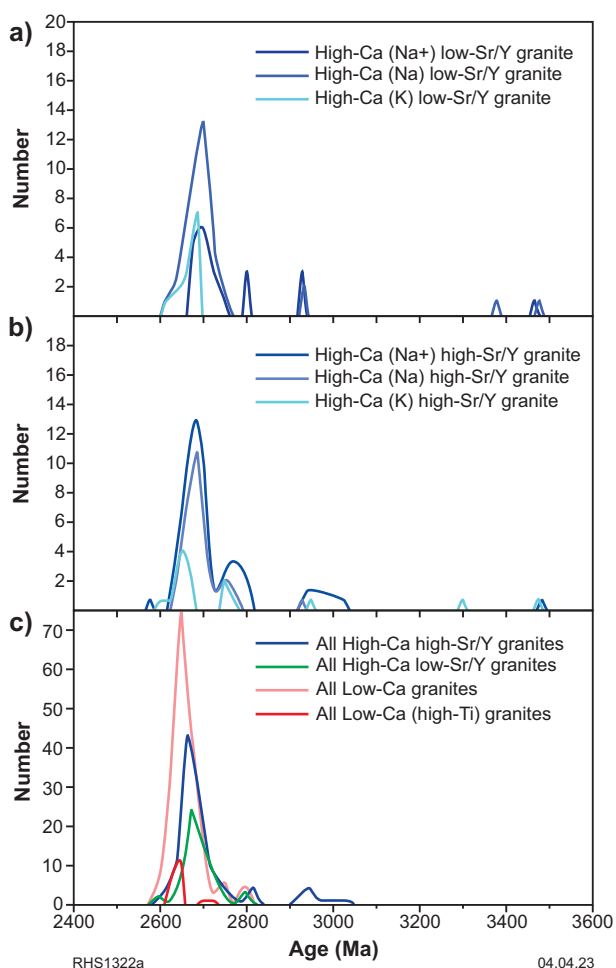


Figure 3. Probability density plot showing the zircon igneous crystallization age distribution for samples of: a) subtypes of High-Ca, low-Sr/Y granites; b) subtypes of High-Ca, high-Sr/Y granites; c) combined High-Ca, high- and low-Sr/Y granites and Low-Ca and Low-Ca (high-Ti) granites <3200 Ma

## High-Ca (high-Sr/Y) granites

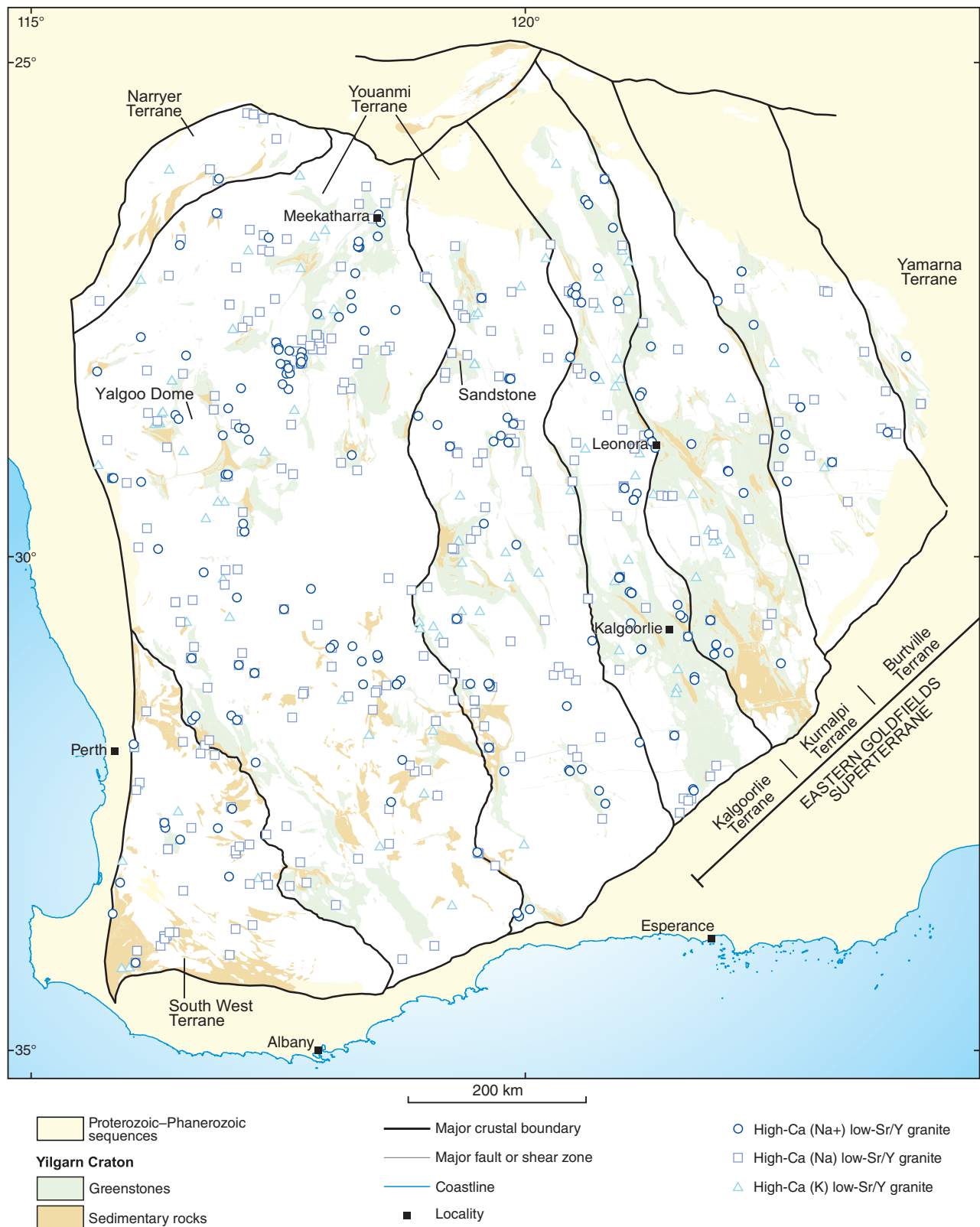
The High-Ca (high-Sr/Y) granite classification is dominated by the Na<sup>+</sup> subgroup (~50%), with relatively few (~12%) potassic samples, although the relative ratio of Na<sup>+</sup>, Na and K subgroups does not significantly change with age. Ages of intrusion range from c. 2605 to 3495 Ma (Fig. 3b), with ages >3290 Ma all coming from the Narryer Terrane, and ages between c. 2990 and 3290 Ma found in all terranes, although predominantly from the Youanmi Terrane (Fig. 6). Major periods of preserved magmatism occur at 2670–2660 Ma (main preserved age range – although the main peak for potassic samples is c. 2650–2640 Ma), 2770–2740 Ma and c. 2950 Ma. Samples from the Narryer Terrane appear to be either very old (>2990 Ma) or very young (<2645 Ma).

High-Ca (high-Sr/Y) granites, and in particular the Na<sup>+</sup> subdivision, appear to have a slightly closer association with greenstone belts or greenstone belt margins than the High-Ca (low-Sr/Y) granites (Fig. 7). The Yalgoo Dome and the area around the settlement of Sandstone are two rare examples of large granitic tracts distal to greenstones where high-Sr/Y varieties outnumber low-Sr/Y varieties (Fig. 7). Like the High-Ca (low-Sr/Y) granites, Na<sup>+</sup> and Na high-Sr/Y subgroups also appear to be strongly associated with major structures, particular in the Youanmi Terrane. Although Na<sup>+</sup> High-Ca (high-Sr/Y) granites are widespread, they are virtually absent (10 samples only) from the central part of the Youanmi Terrane and the northern South West Terrane (Fig. 8a). This region also has a particularly low density of Na High-Ca (high-Sr/Y) granites (Fig. 8b). Thus, the distribution of Na<sup>+</sup> High-Ca (high-Sr/Y) granites in the Youanmi Terrane appears to define two regional-scale blocks, an easterly trending zone forming approximately the northern half of the terrane (northern Youanmi Terrane high-Sr/Y granite zone), and a northeast-trending zone along the southeastern part of the terrane (southern Youanmi Terrane high-Sr/Y granite zone) (Smithies et al., 2019) (Fig. 8b).

A high concentration of High-Ca (high-Sr/Y) granites lie within the Cue isotopic zone of the Youanmi Terrane and in the EGST (Fig. 7). In both regions, a large proportion of the Na<sup>+</sup> and Na subgroups lie within or are marginal to greenstone belts or appear closely related to major structures that influence greenstone distribution.

In the Cue isotopic zone, the various subgroups of High-Ca (high-Sr/Y) granites are spatially associated with greenstones, although their spatial distribution appears otherwise broadly random. High-Ca granites (high- and low-Sr/Y) with magmatic zircon crystallization ages representing the younger (2730–2610 Ma) of the three broad magmatic periods recorded within the northern Youanmi Terrane (i.e. 3000–2900, 2820–2740 and 2730–2610 Ma) appear to define a central northern axial core to the Cue isotopic zone (Fig. 6). The full compositional range of High-Ca granites is represented within the core of the zone, and also with the surrounding regions of dominantly older granites.

In the EGST, in particular, the distribution of Na<sup>+</sup> High-Ca (high-Sr/Y) granites defines a series of northwest (~320°) trends that parallel the structural trend of the greenstones and many of the greenstone-bounding faults (Figs 7, 8a).

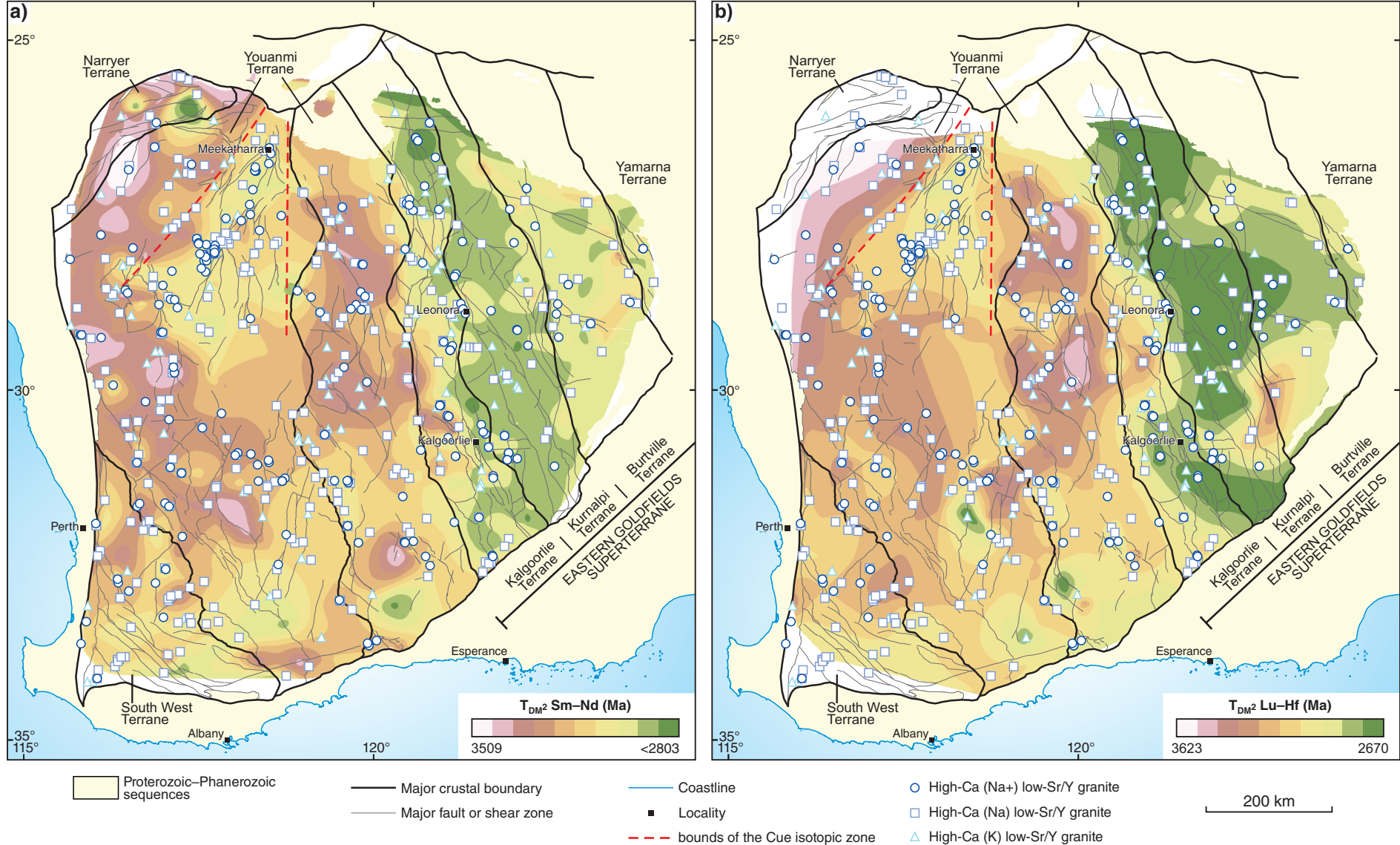


RHS1313a

13.01.23

Figure 4. Summarized bedrock geology of the Yilgarn Craton showing the distribution of High-Ca, low-Sr/Y granites

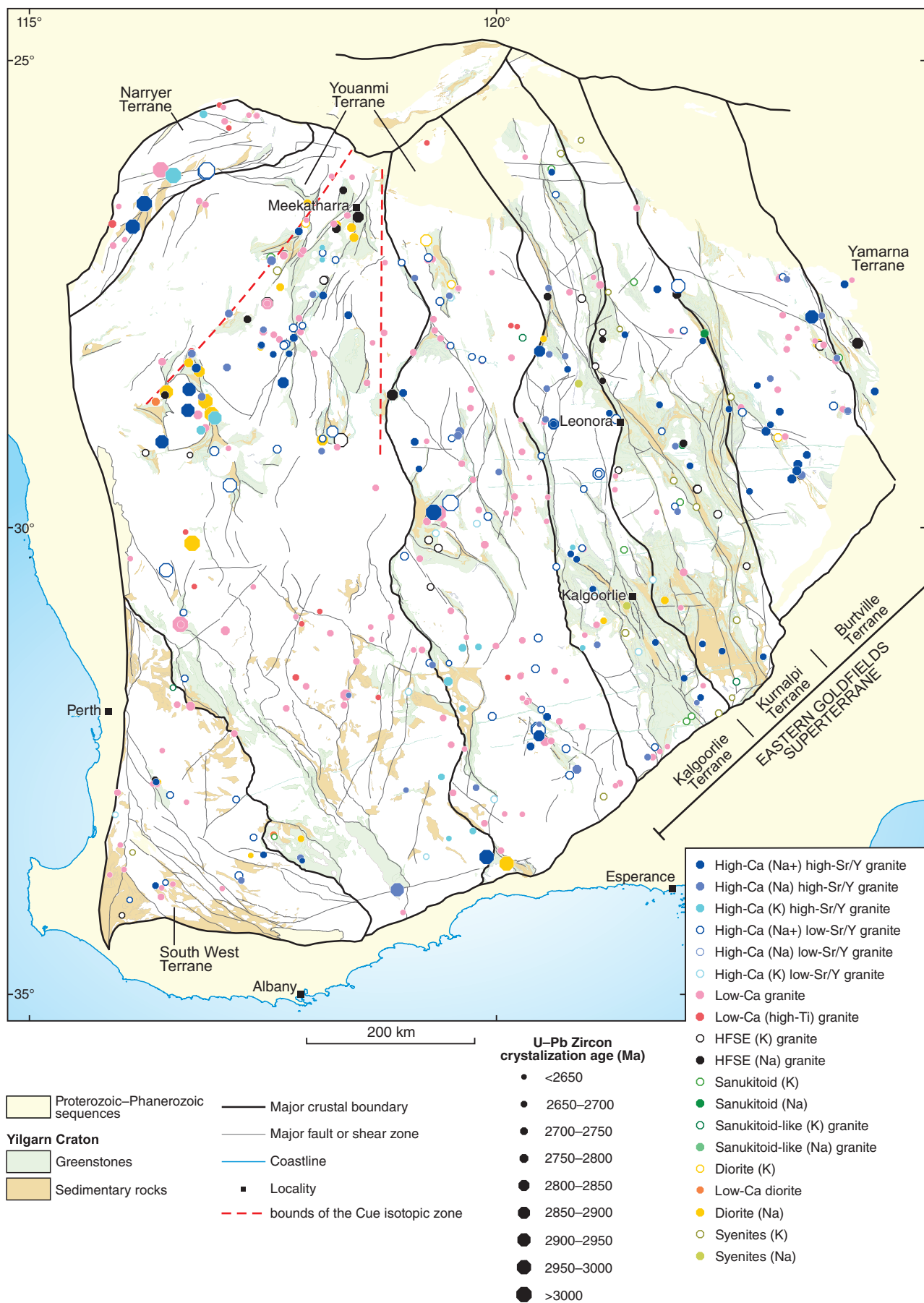




RHS1313j

04.04.23

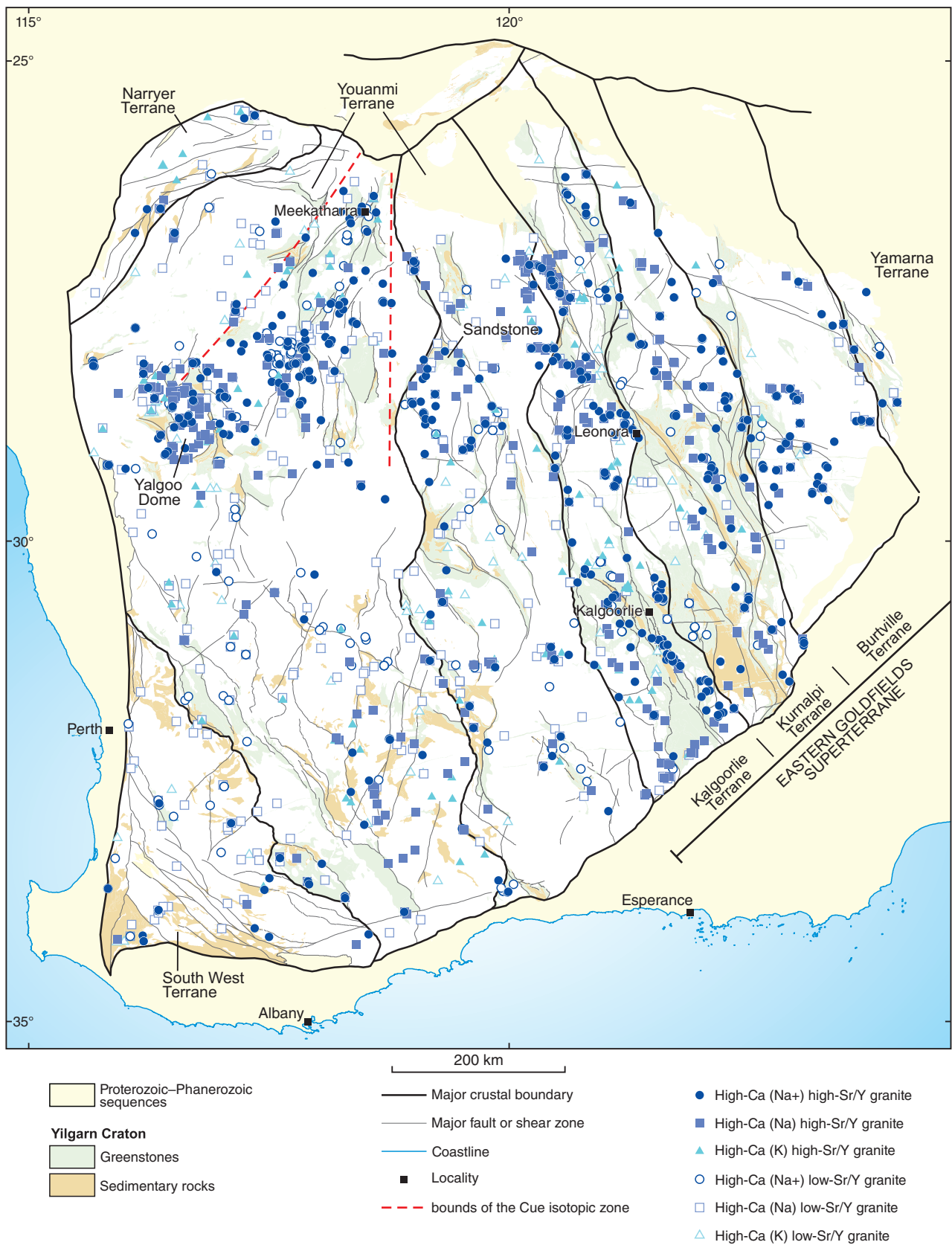
Figure 5. Regional outline of the Yilgarn Craton overlaying the distribution of High-Ca, low-Sr/Y granites on contour maps showing variations in model ages ( $T_{DM^2}$ ) from: a) Sm-Nd isotope measurements; b) Lu-Hf isotope measurements (isotope data from Lu et al., 2021a,b)



RHS1315a

04.04.23

Figure 6. Summarized bedrock geology of the Yilgarn Craton showing zircon igneous crystallization age and distribution, and classification of granite samples



RHS1313I

13.01.23

Figure 7. Summarized bedrock geology of the Yilgarn Craton showing the distribution of all High-Ca granites



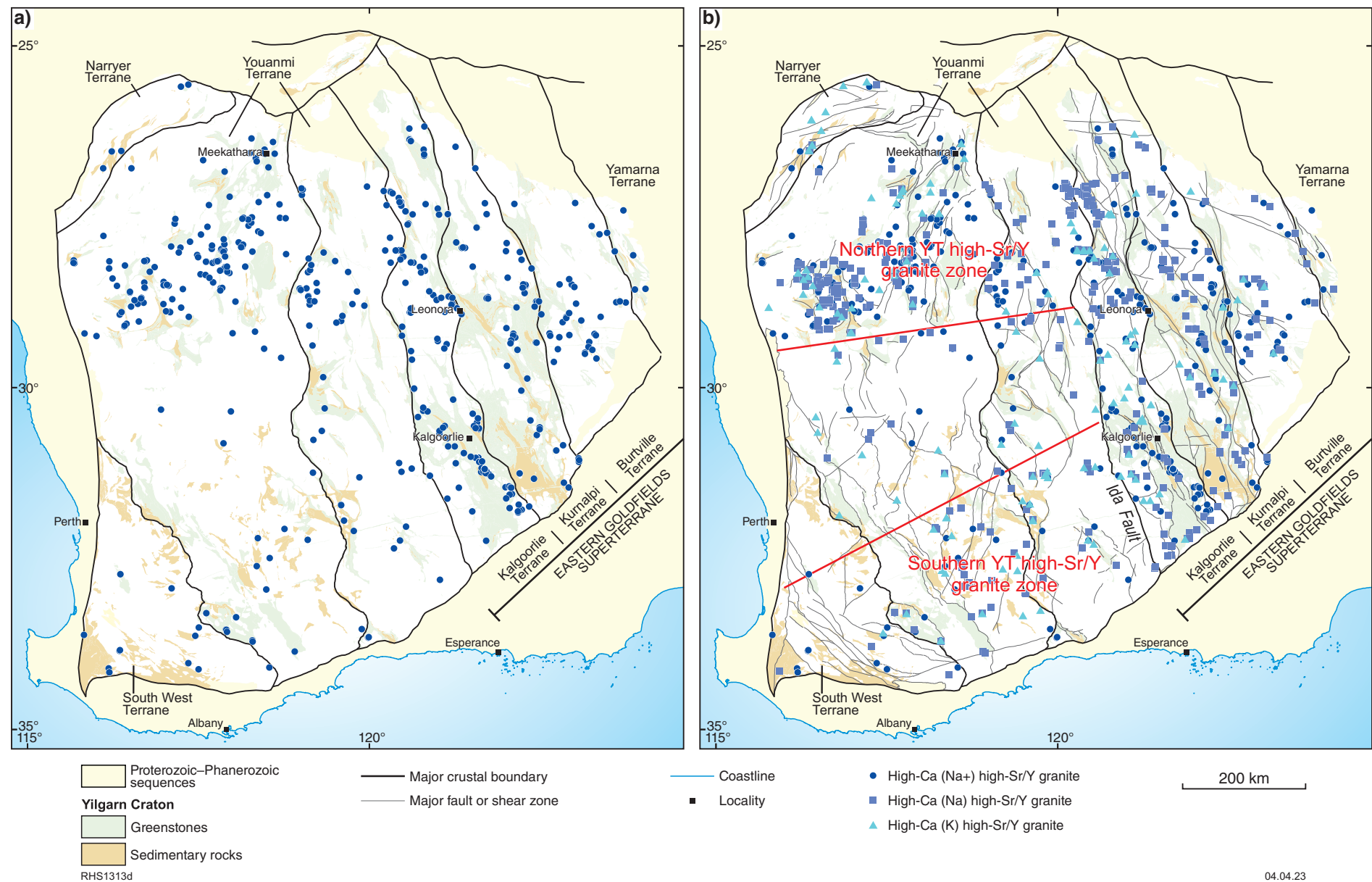


Figure 8. Summarized bedrock geology of the Yilgarn Craton showing the distribution of: a) High-Ca (Na<sup>+</sup>), high-Sr/Y granites; b) all High-Ca, high-Sr/Y granites



In the Kalgoorlie region, for example, a distinct northwest trend in Na<sup>+</sup> High-Ca (high-Sr/Y) granites can be traced for up to 230 km. Na<sup>+</sup> High-Ca (high-Sr/Y) granites also define a northerly trend near the western margin of the EGST, although this does not coincide with the Ida Fault in all places (Fig. 8a). Both the northwest and northerly trends are further accentuated by the Na, but not so clearly by the K, subgroups of High-Ca (high-Sr/Y) granites. High-Ca (high-Sr/Y) granites contributing to these trends in the EGST are almost all <2700 Ma in age, and there is considerable overlap in the spatial and temporal distribution of high- and low-Sr/Y High-Ca granites.

## Low-Ca granites

Low-Ca granites are the most common granite group identified, forming approximately 30% of our dataset. They are distributed throughout the craton but are slightly less common in the southern part of the South West and Youanmi Terranes and throughout the EGST (Fig. 9). They tend to form fewer intrusions into greenstones than do the High-Ca granites (and particularly the high-Sr/Y High-Ca subgroups) despite a slightly younger peak (2660–2650 Ma; Fig. 3c) in their zircon crystallization age distribution relative to other granite groups. Although in regions such as the central and southern Youanmi Terrane the spatial distribution of the Low-Ca granites appears relatively even, in other areas, there is a spatial association with major faults (Fig. 9). This particularly appears to be the case with those Low-Ca granites with higher magmatic temperatures of intrusion (as estimated by the zircon saturation temperature,  $T_{\text{zircon}}$  °C; Watson and Harrison, 1983) (Fig. 10). Hence, as a generalization, Low-Ca granites with high  $T_{\text{zircon}}$  commonly intrude along major or crustal-scale faults whereas Low-Ca granites commonly form components of batholithic bodies between structures and/or greenstones and typically have lower  $T_{\text{zircon}}$  (typically <800 °C). An exception to this is a zone or group of high  $T_{\text{zircon}}$  Low-Ca granites close to the northwestern and southwestern margins of the Youanmi Terrane, adjacent to the Narryer and South West Terranes. These are associated with Low-Ca (high-Ti) granites and will be discussed later.

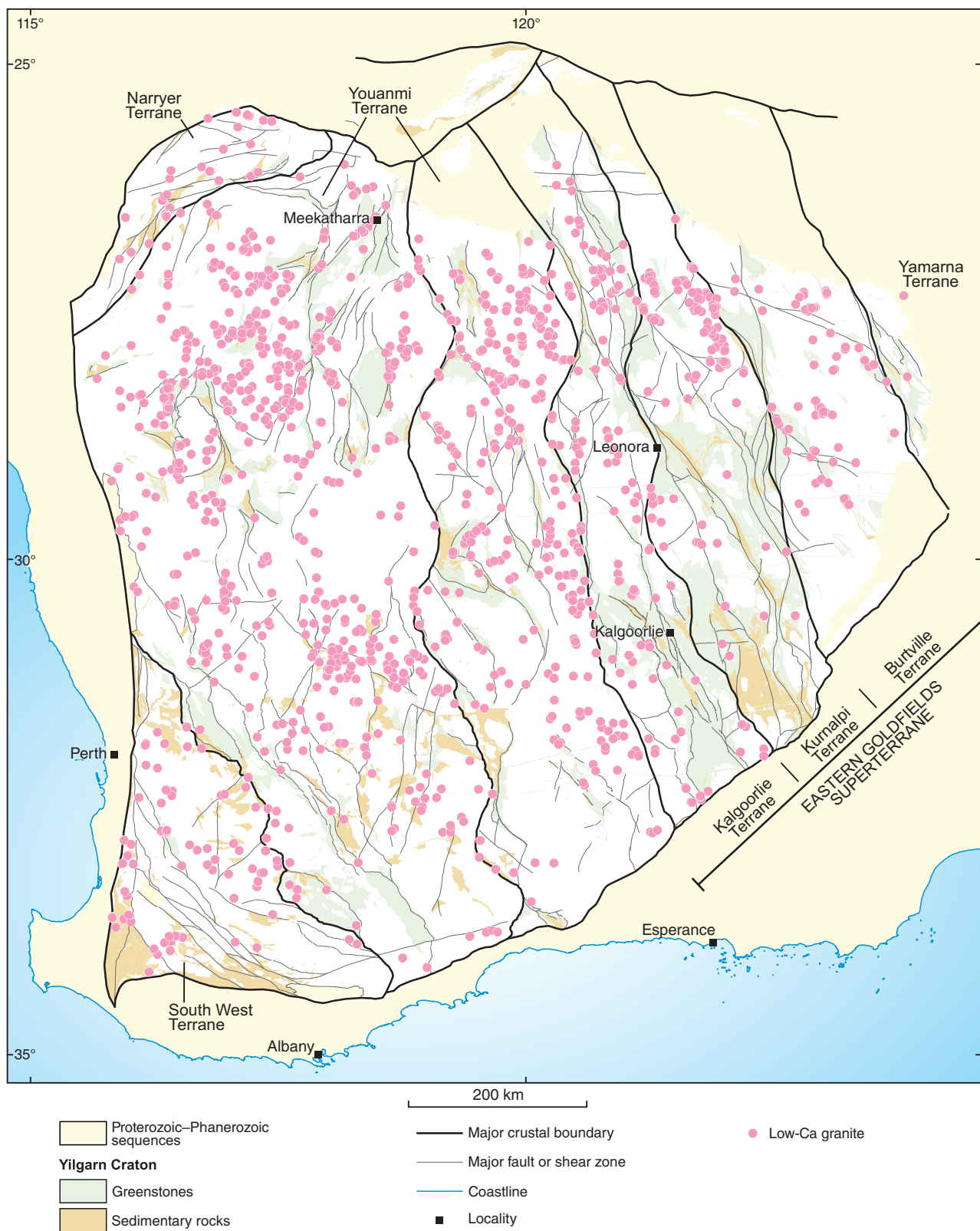
Within and adjacent to the EGST, Low-Ca granites also tend to occur along discrete trends, both north and northwest (Fig. 10b). Here, progressively removing samples with the lowest magmatic temperature first removes all of the northwest trends, leaving only samples (with  $T_{\text{zircon}}$  >820 °C) approximating the northerly striking faulted boundary between the Youanmi Terrane and the EGST (in places corresponding with the Ida and Ballard Faults) (Fig. 11). On a regional scale, there is a contrast in dominant granite type across this trend, with Low-Ca to the west, Na<sup>+</sup> and Na High-Ca (high-Sr/Y) to the east (Figs 2, 10a). There is also a northerly trending group of Low-Ca granites with high  $T_{\text{zircon}}$  in the northeastern part of the Kurnalpi Terrane, northeast of the Dukton greenstone belt, that does not correspond to any feature currently recognized at the surface as a major fault (Fig. 10). We speculate that this might reflect a cryptic expression of part of the northern boundary between the Kurnalpi and Burtville Terranes.

Low-Ca granites with ages >2750 Ma are rare and mainly occur in the Narryer Terrane (samples as old as c. 3680 Ma) or the northwestern and western parts of the Youanmi Terrane (Figs 3c, 6). Most samples with ages >2680 Ma are also concentrated in these regions. The remaining samples, with ages between 2685 and 2606 Ma, comprise >75% of the dated population and show no apparent systematic geographical distribution other than those described above. There is, however, a significant regional variation in  $T_{\text{DM}}^2$  ages of the 2685 to 2606 Ma Low-Ca granites, reflecting regional variations in bulk average source age (Fig. 12). The Narryer Terrane is overwhelmingly dominated by  $T_{\text{DM}}^2$  ages >3350 Ma, the Youanmi and South West Terranes are overwhelmingly dominated by  $T_{\text{DM}}^2$  ages between 3350 and 2950 Ma (samples from the Cue isotopic zone at the younger end of that range), with very rare occurrences of ages >3400 Ma, whereas the EGST is overwhelmingly dominated by  $T_{\text{DM}}^2$  ages <3010 Ma, with very rare occurrences of ages up to 3090 Ma.

## Low-Ca (high-Ti) granites

These form a new subgroup of Low-Ca granites, with anomalously high TiO<sub>2</sub>, P<sub>2</sub>O<sub>5</sub>, and rare earth element and Zr concentrations, reflecting higher temperature melting of a drier and more refractory source than that of normal Low-Ca granite. Although these share some transitional compositional characteristics with both HFSE granites and syenites, they are typically not strongly associated spatially with either, particularly in the EGST (Fig. 2). Low-Ca (high-Ti) granites are, however, strongly associated spatially with the main Low-Ca granite group, particularly in areas where the Low-Ca granites also show high  $T_{\text{zircon}}$  values, typically distal to greenstone belts (Figs 9–11). Such regions include the western margin of the Youanmi Terrane, including the northern and central part of its newly reinterpreted boundary with the South West Terrane, and along both the western margin of the EGST and the northeastern region of the Kurnalpi Terrane (Quentin de Gromard et al., 2021). Low-Ca (high-Ti) granites are virtually absent from the Kalgoorlie and Kurnalpi Terranes of the EGST and from the central region of the Youanmi Terrane. Nearly all existing U–Pb zircon crystallization ages from Low-Ca (high-Ti) granites lie between c. 2655 and c. 2610 Ma, typically within the younger part of the range for Low-Ca granite (Fig. 3c).

In the western marginal zone of the Youanmi Terrane, and including the Narryer Terrane to the northwest, Low-Ca (high-Ti) granites are associated with abundant Low-Ca granites, forming a distinct zone from the South West Terrane boundary and extending up to 200 km into the Youanmi Terrane (Fig. 10b). Although Low-Ca granite occurs east and west of the South West Terrane boundary, these are not accompanied by large numbers of Low-Ca (high-Ti) granites. Normal Low-Ca granites within this zone are compositionally indistinguishable from those elsewhere in the craton and mostly lie within the same <2700 Ma age population. However, where determined, normal Low-Ca granites within this zone have higher  $T_{\text{DM}}^2$  ages (typically >3250 Ma) (Figs 12, 13) and correspondingly lower initial  $\epsilon_{\text{Nd}}$  (Fig. 14) than all other Low-Ca granites except for a group of samples close to the boundary between the Youanmi Terrane and the EGST.



RHS1313h2

13.01.23

Figure 9. Summarized bedrock geology of the Yilgarn Craton showing the distribution of all Low-Ca granites

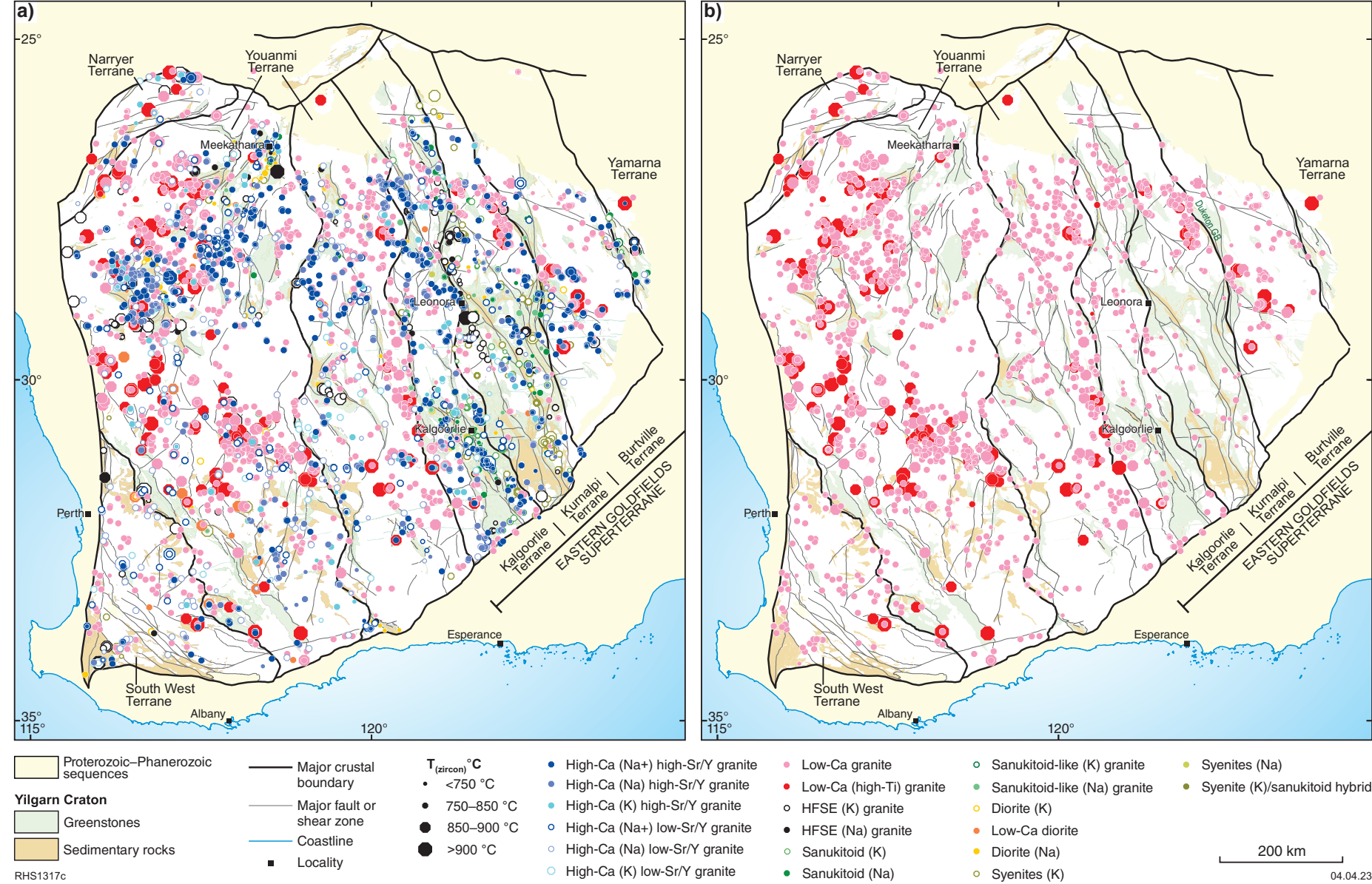
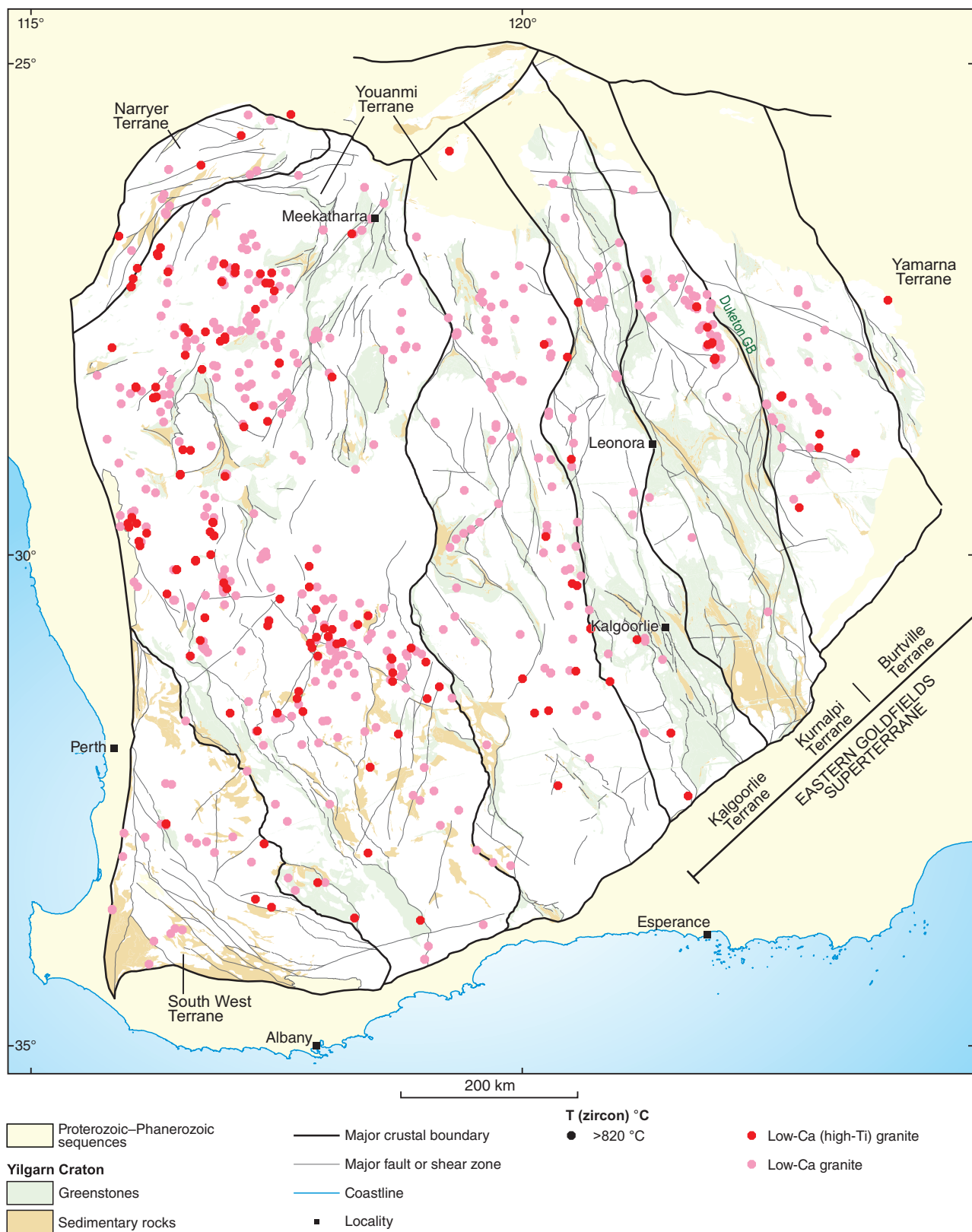


Figure 10. Summarized bedrock geology of the Yilgarn Craton showing the calculated zircon saturation temperature [ $T_{\text{zircon}} (^{\circ}\text{C})$ ] for: a) all samples; b) Low-Ca granites and Low-Ca (high-Ti) granites



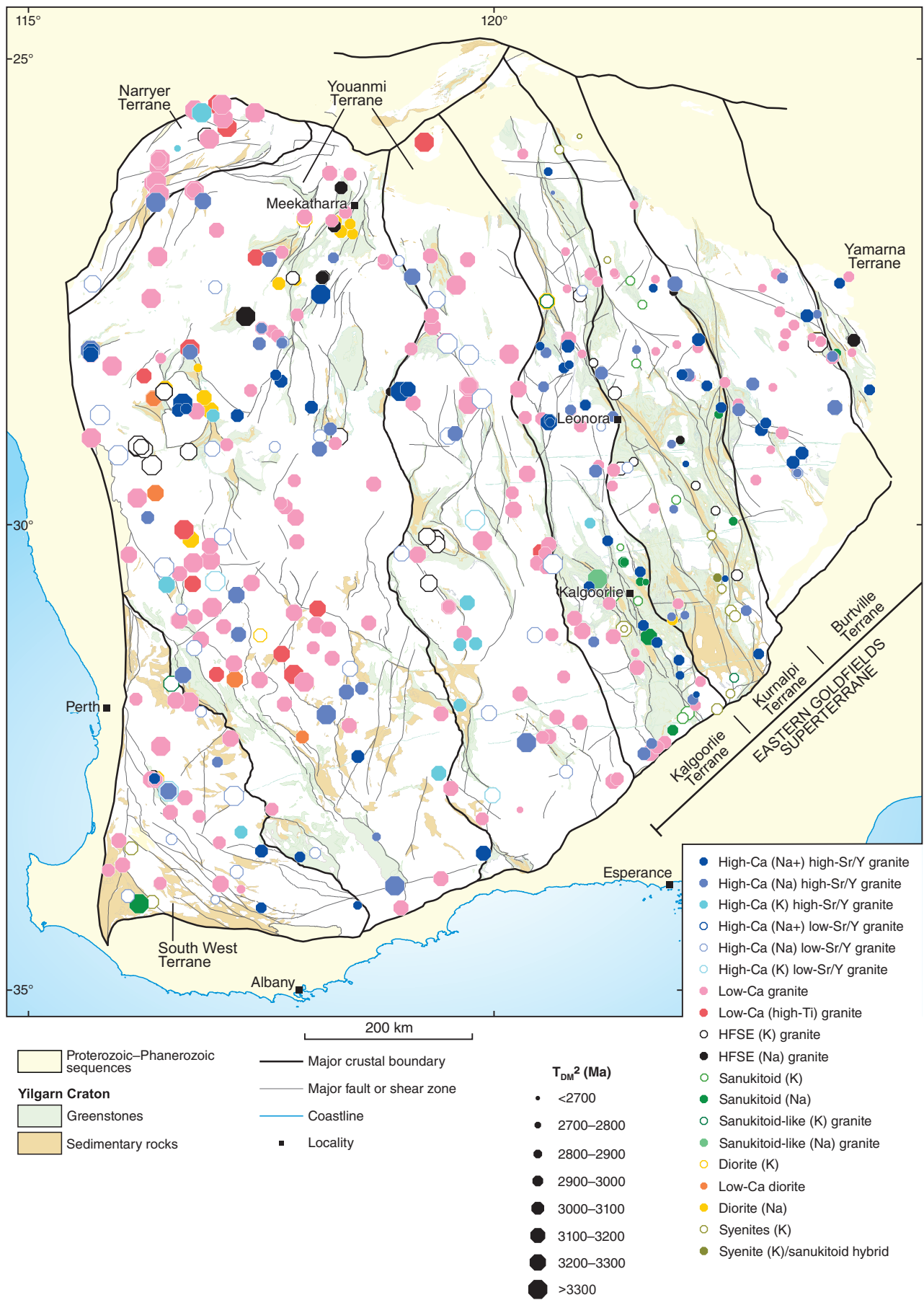


RHS1317b

13.01.23

Figure 11. Summarized bedrock geology of the Yilgarn Craton showing the distribution of Low-Ca granites and Low-Ca (high-Ti) granites with calculated zircon saturation temperatures [ $T_{\text{zircon}} \text{ } ^\circ\text{C}$ ] >820 °C

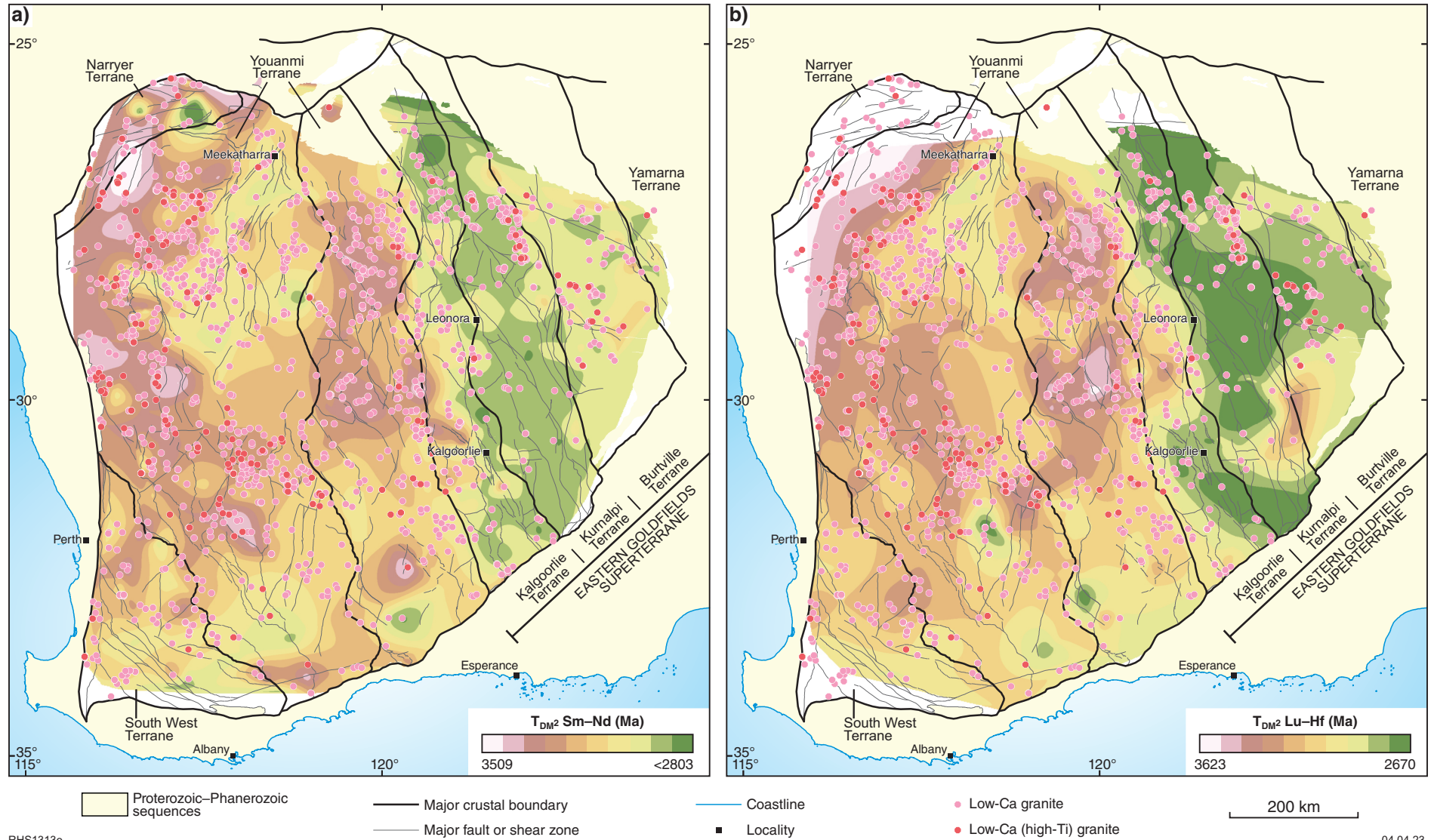




RHS1314

13.02.23

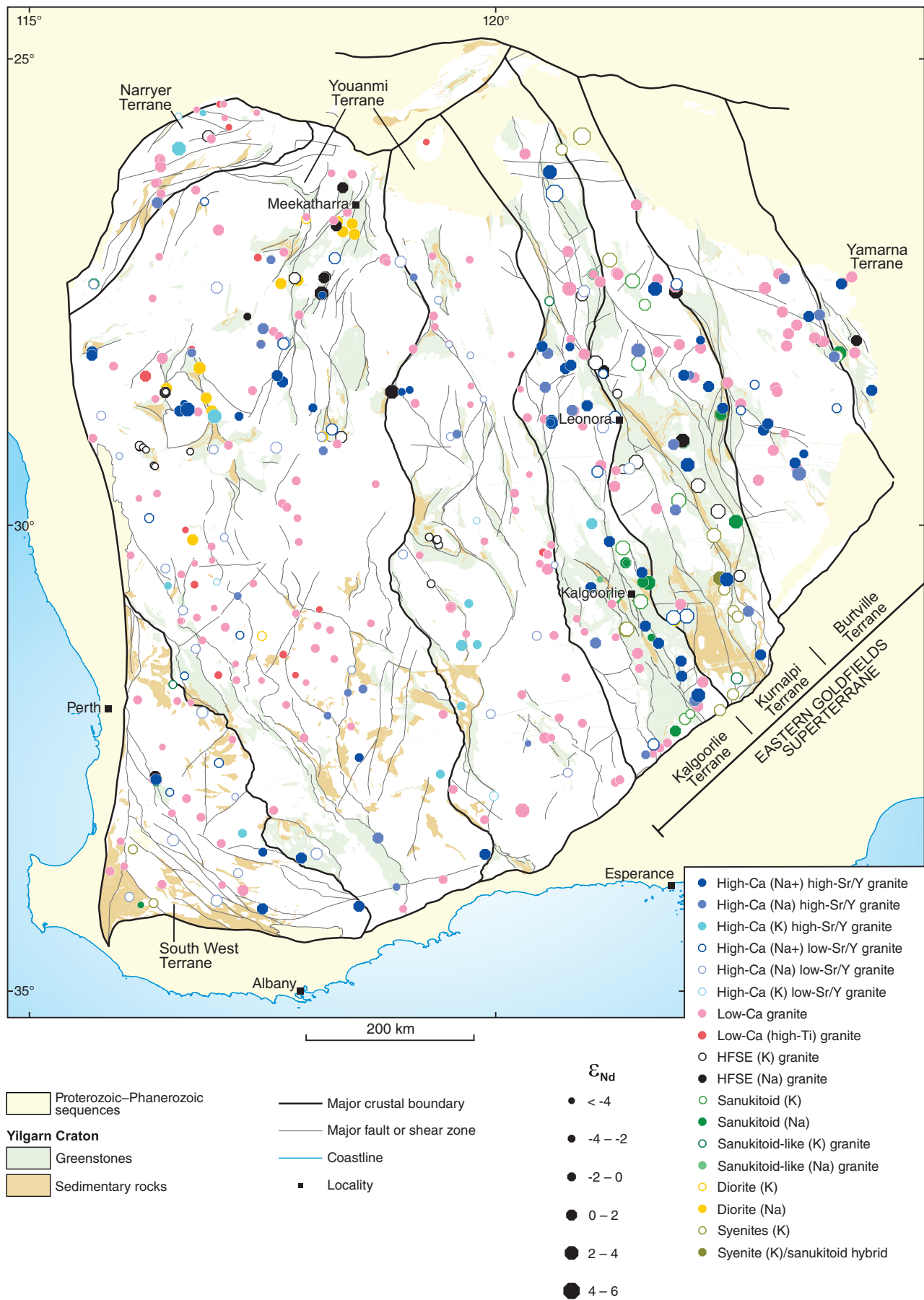
Figure 12. Regional outline of the Yilgarn Craton showing the spatial distribution of all samples for which Nd-isotope data are available and model ages ( $T_{DM}^2$ ) derived from those data (isotope data from Lu et al., 2021a,b)



RHS13130

04.04.23

Figure 13. Distribution of Low-Ca granites and Low-Ca (high-Ti) granites on contour maps showing variations in model ages ( $T_{DM2}$ ) from: a) Sm-Nd isotope measurements; b) Lu-Hf isotope measurements (isotope data from Lu et al., 2021a,b)



RHS1316a

13.02.23

Figure 14. Summarized bedrock geology of the Yilgarn Craton showing the spatial distribution of all samples for which Nd-isotope data are available and initial  $\epsilon_{Nd}$  values derived from those data (isotope data from Lu et al., 2021b)



In contrast to the granites forming the Low-Ca (high-Ti) granite zone in the western Youanmi Terrane, Low-Ca (high-Ti) granite, and associated normal Low-Ca granites with high  $T_{\text{zircon}}$  in the Duketon area of the EGST and those occurring near the northern part of the Kurnalpi/Burtville Terrane boundary (Fig. 10), are considerably more focused into narrow belts, likely reflecting a strong structural control. They probably reflect more efficient channelling of hot, dry magmas along major crustal structures.

## High field strength element granites

HFSE granites occur in small numbers throughout the Yilgarn Craton (Fig. 15). Primitive examples mostly have clear tholeiitic compositions (Fig. 16) and most of the more evolved examples have compositions expected of evolved tholeiites. Distinctive enrichments in HFSE and in heavy rare earth elements (HREE) (including elevated and flat mantle-normalized HREE patterns) are also features typical of evolved tholeiitic magmas, including A-type granites associated with tholeiitic liquid lines of descent or high-temperature melting of dry tholeiitic basalt. The HFSE granites mainly occur within, or marginal to, greenstone belts and/or major structures (Fig. 15). The Na-rich HFSE granites (i.e.  $K_2O/Na_2O < 0.6$ ) show a greater tendency to intrude within greenstone sequences; samples with the least radiogenic Nd tend to be K rich, suggesting that contamination by evolved lower crust is more likely away from greenstone belts and is a factor in determining the  $K_2O/Na_2O$  of the HFSE granites. HFSE granites are more common in the northern part of the craton, particularly in the Cue isotopic zone and the northern EGST.

In the Cue isotopic zone, Na-rich HFSE granites are concentrated within the axial zone, whereas K-rich HFSE granites are more regionally spread (Fig. 15). Immediately to the south of the Yalgoo Dome, K-rich HFSE granites form a distinct easterly trending zone, 100 km long, within the northern portion of a similarly trending zone of large overlapping 'nested' intrusions (Fig. 15). The HFSE granites appear to lie within greenstones, and granites forming country-rock to these late granites mainly include high-K low- and High-Ca granites.

HFSE granites in the EGST define regional trends with a high degree of linearity (Fig. 15). The most extensive of these trends – forming the HFSE-N1 belt – extends for approximately 200 km along the Keith-Kilkenny and Melita-Emu fault systems, or nearby splays, and forms the largest and most southwesterly member of a set of three west-northwesterly trending en-echelon HFSE granite belts (HFSE-N1–3). The western two belts (HFSE-N2 and N3) intersect the established boundary fault (Ockerburry Fault) separating the Kalgoorlie and Kurnalpi Terranes. To the south, HFSE-N1 appears to intersect HFSE-E and terminates close to a northwest-trending line of syenite and sanukitoid intrusions (see below). Other potential trends are shown in Figure 15 and include a series of intrusions (KaHFSE-S) that broadly coincide with a northwest-trending ( $\sim 320^\circ$ ) zone of sanukitoids and syenites in the southern Kalgoorlie Terrane (KaSa-S – see below), and several intrusions along both the old (SW-YT-old) and recently reinterpreted (SW-YT-new) boundary between the South West Terrane and Youanmi Terrane.

Available dating includes rare samples with U–Pb zircon crystallization ages  $> 2800$  Ma (Fig. 17) scattered across the northwestern part of the craton and in the far east (Yamarna Terrane; Fig. 6). Na-rich HFSE granites in the axial zone of the Cue isotopic zone have igneous crystallization ages mainly (four out of six dates) between 2739 and 2746 Ma, but older ages of c. 2782 and 2806 Ma are also recorded. Two K-rich HFSE granite samples included within the easterly trending belt south of the Yalgoo Dome have igneous crystallization ages of c. 2670 and c. 2631 Ma. All dated samples from the Kalgoorlie and Kurnalpi Terranes lie within a broad range between c. 2750 and c. 2630 Ma. Nearly all HFSE granites are older than nearly all syenites and most sanukitoids (Fig. 17). Not enough age data exists to fully constrain the periods over which any of the various HFSE trends or belts formed; however, the available data provide the following constraints: HFSE-W 2631–2670 Ma, HFSE-E 2681–2714 Ma, HFSE-N1 2686–2692 Ma, HFSE-N2 2658–2738 Ma.

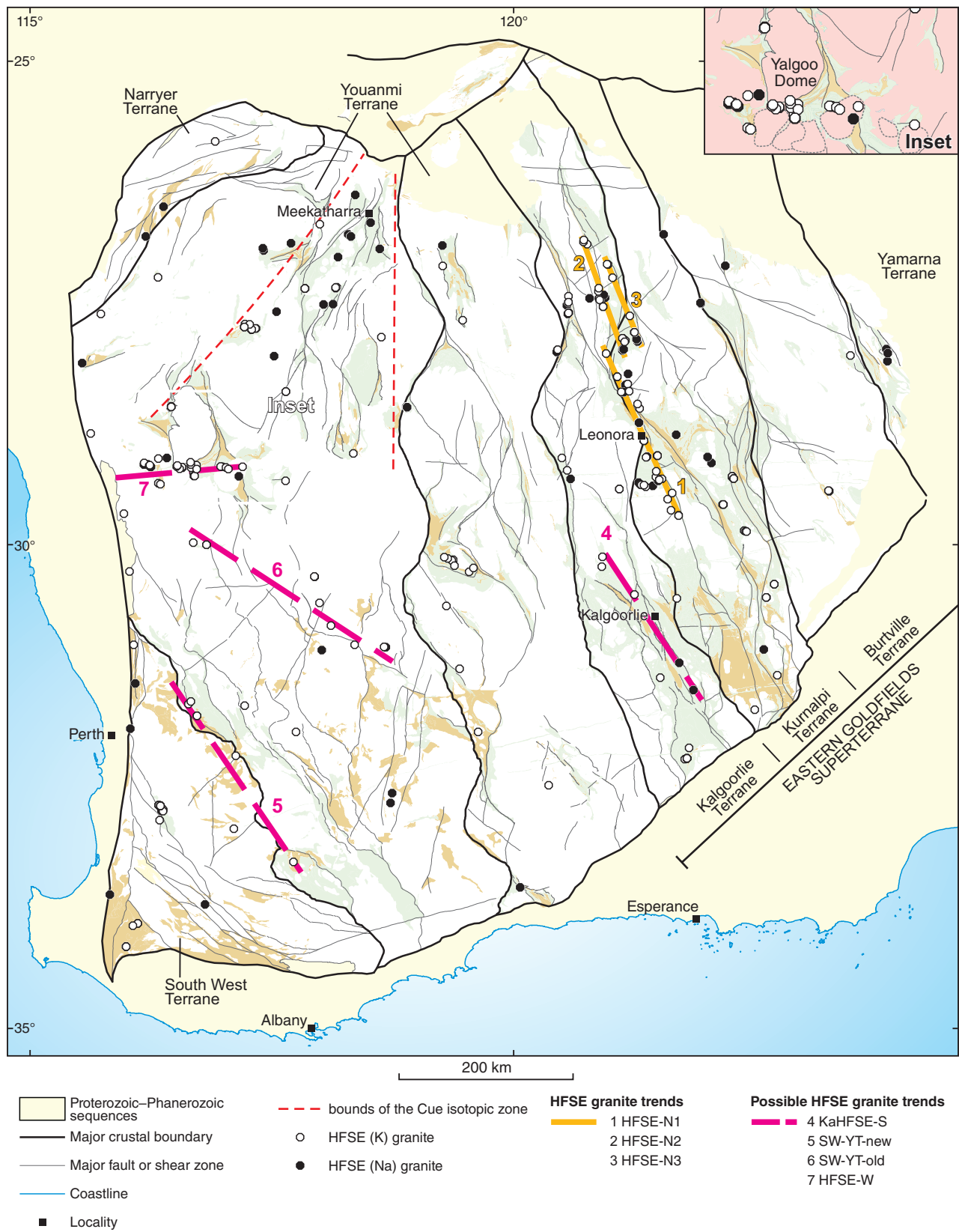
## Syenites

These are the only major Archean rock group of the Yilgarn Craton that fall entirely within the 'alkaline magma series' in terms of their position on a total alkalis-silica (TAS) diagram (Fig. 18), although none of the felsic groups comprise strictly 'alkaline rocks' in terms of having excess molecular Na+K over Al or Si (i.e. none is silica under saturated or otherwise peralkaline, e.g. Shand, 1922). Syenites (here including alkali granites; Fig. 18) are scattered in low numbers throughout the craton but are largely absent in the southern and central Youanmi Terrane (Fig. 19a). Although both K- and Na-syenites occur in the EGST, Na-syenites are absent from the Youanmi Terrane and South West Terrane. In the EGST, K-syenite dominates over Na-syenite and there is a greater tendency for Na-syenites to intrude greenstone belts or structures within or marginal to greenstone belts, particularly close to where Na-sanukitoids are found. In contrast, a high proportion of K-syenites have intruded granitic bodies between greenstone belts. Despite the high apparent magmatic temperatures of many of the syenites (Fig. 10a) – as indicated by their high  $T_{\text{zircon}}$  values ( $> 840^\circ\text{C}$  in many cases) – the distribution of syenites and of Low-Ca (high-Ti) granites appears mutually exclusive. The range in U–Pb zircon crystallization age for rocks classified as syenite is between c. 2744 and 2629 Ma but about 75% of samples (11 of 15) lie between c. 2670 and 2640 Ma (Fig. 17b).

## Sanukitoids

Apart from a few scattered occurrences within the South West Terrane, sanukitoids are essentially restricted to the EGST and to the Cue isotopic zone in the northern Youanmi Terrane (Fig. 19b). In these regions the distribution of sanukitoids closely matches that of the Na+ High-Ca (high-Sr/Y) granites, likewise locally defining similar northwest-trending lines or zones of intrusions (c.f. Figs 8a, 19b). Most sanukitoids form intrusions into greenstone sequences or volcanic rocks deposited over greenstone sequences. However, compared to Na-sanukitoids, at least within the EGST, a higher proportion of K-sanukitoids intrude, or form phases within, granitic regions between greenstones.





RHS1313m

15.02.23

Figure 15. Summarized bedrock geology of the Yilgarn Craton showing the distribution of high-HFSE granites and possible arrays of high-HFSE granites

The available U–Pb zircon crystallization age data on rocks classified here as either syenite or sanukitoid shows that their magmatic age range is indistinguishable (Fig. 17). Thus, apart from single magmatic crystallization ages at 2960 Ma in the northern EGST and 2716 Ma nearby in Duketon region, and two ages at c. 2750 Ma in the Cue isotopic zone, the magmatic age range for rocks classified as sanukitoid is between c. 2700 and 2644 Ma with approximately 90% of the population between c. 2680 and 2644 Ma.

### Spatial relationships and trends between sanukitoids and syenites

In the Cue isotopic zone, the distribution of sanukitoids overlaps that of K-syenites forming a broad northeasterly trending belt. Within that broad region, Na-sanukitoids appear more abundant in the east and K-sanukitoids in the west (Fig. 19).

There is a strong spatial relationship between sanukitoids and syenites in the Kalgoorlie and Kurnalpi Terranes of the EGST, with several north-northwesterly trending ‘belts’ of intrusions incorporating either or both sanukitoids and syenites (Fig. 20). At many specific locations within these belts, both sanukitoid and syenite are found. Whereas this is consistent with the available dating suggesting that the periods of sanukitoid magmatism and syenite magmatism largely overlapped on a regional basis, where direct intrusive relationships are observed, syenites typically post-date sanukitoids. At several sites (e.g. Carasue Dam, Wallaby), syenites have compositions that overlap those of sanukitoids for most elements (but have higher  $\text{Na}_2\text{O} + \text{K}_2\text{O}$ ) and might have hybrid compositions. Virtually all Na-syenites from the southern Kurnalpi Terrane, and several from the southern Kalgoorlie Terrane, are notably depleted in  $\text{Al}_2\text{O}_3$  (<16 wt%; and most of these have higher MgO) and have other compositional traits strongly resembling Na-sanukitoid or a Na-sanukitoid/syenite hybrid.

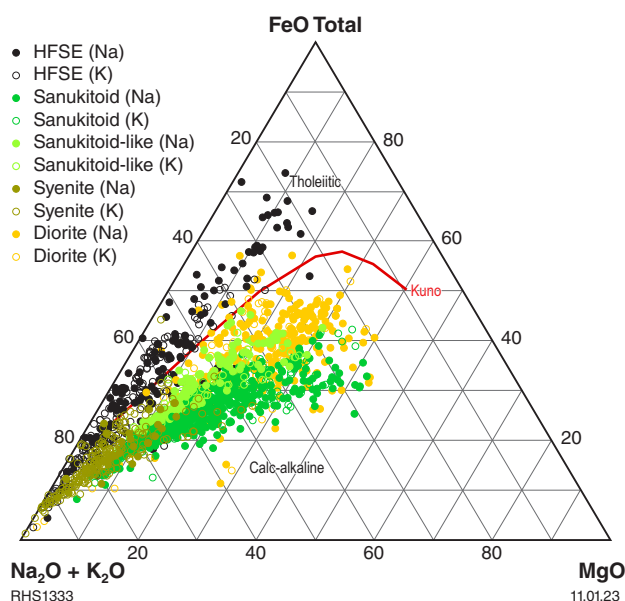


Figure 16. AFM diagram showing where various granite classes plot with respect to the calc-alkaline – tholeiite compositional boundary of Kuno (1968)

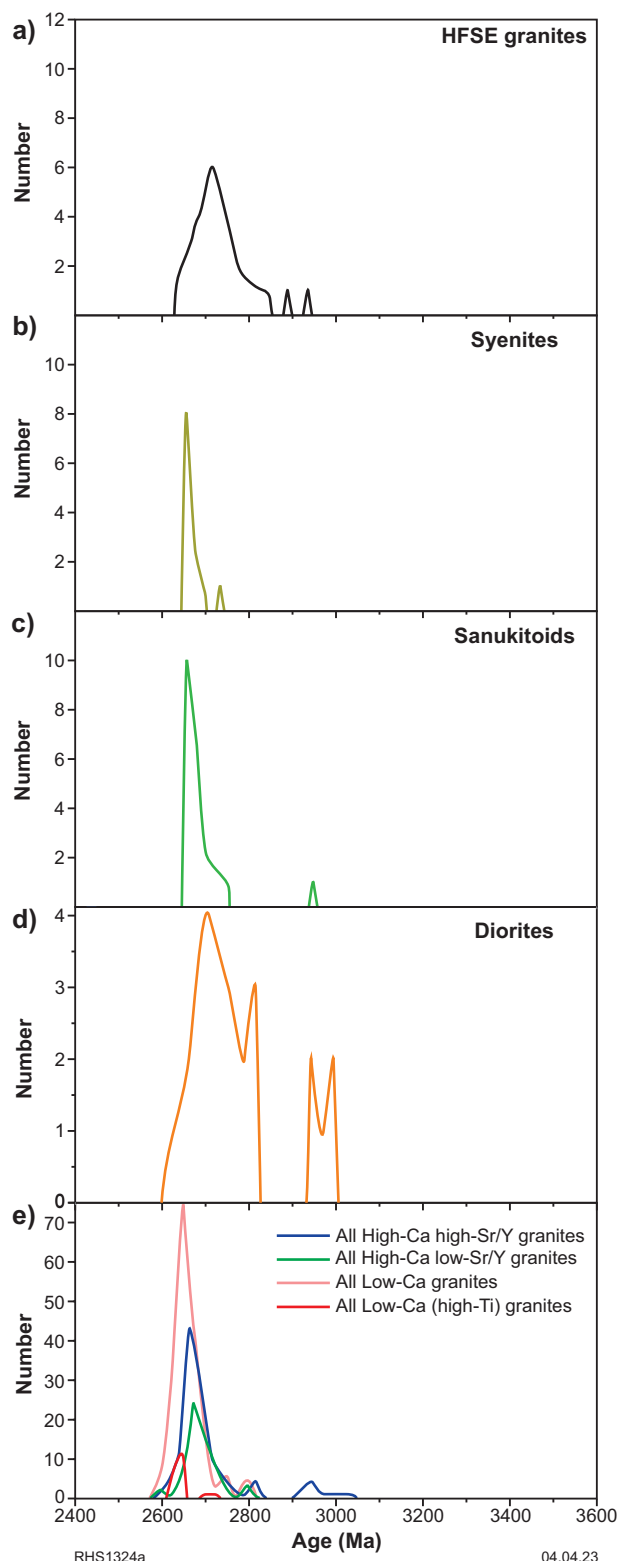


Figure 17. Probability density plot showing the zircon igneous crystallization age distribution for samples of: a) high-HFSE granites; b) syenites; c) sanukitoids; d) diorites; e) comparing these with the age distribution probability density plot for the major granite types

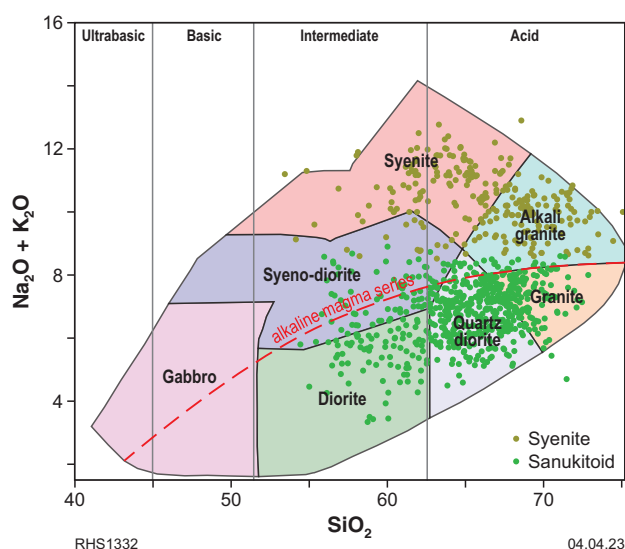


Figure 18. TAS diagram (modified after Cox et al., 1979) showing the distribution of syenites and sanukitoids

Because of the strong spatial relationship that syenites and particularly sanukitoids have with greenstone belts, it can be argued that the extent and orientation of these intrusions simply reflect the extent of greenstone outcrop and the structural controls on that outcrop. However, there are also very large areas of greenstone outcrop where few, if any, sanukitoids have been identified. In addition, a direct relationship between the emplacement of mantle-derived sanukitoids and major faults (mantle-tapping systems) has clearly been established (e.g. Perring et al., 1989; Witt et al., 2013, 2015; Smithies et al., 2018c).

The interpreted boundaries or extent of several of the sanukitoid/syenite belts is influenced by their relationship with structures interpreted to reflect the boundary between the Kalgoorlie and Kurnalpi Terranes: several belts (e.g. KaSa-NW; Fig. 20) could potentially be extended to cut that boundary. Whereas sanukitoids and syenites occur throughout both terranes, from a regional perspective, the Kalgoorlie Terrane appears to be sanukitoid-dominated ( $\text{Na} > \text{K}$  c.f.  $\text{K} > \text{Na}$  in the Kurnalpi Terrane) and the Kurnalpi Terrane appears to be syenite-dominated.

A broad belt (KaSa-S; Fig. 20) with more sanukitoids than syenites extends between Norseman and Ora Banda in the southern part of the Kalgoorlie Terrane. Sanukitoids in this belt are dominantly Na-sanukitoids and syenites are dominantly K-syenites. The belt nevertheless contains the highest density of Na-syenites within the Yilgarn Craton.

A more constrained belt with considerably more syenites than sanukitoids (KuSy-S) lies within the Kurnalpi Terrane. This belt includes the Erayinia Granite in the south and continues northwards for over 160 km, with intrusions in and peripheral to the Keith-Kilkenny Fault. This belt is overwhelmingly dominated by K-syenites, contains no Na-syenites, rare sanukitoid/syenite hybrids, and only few sanukitoids, most of which are K-sanukitoids (including primitive sanukitoid from Carasue Dam).

The KaSa-S and KuSy-S belts terminate along a less well-constrained, northeast-trending zone locally also marked by syenite and sanukitoid intrusions (Fig. 20). In the region between this northeast-trending zone and northwards to the Leonora region, both syenite and sanukitoid intrusions are more scattered and mainly potassic.

Further to the northwest a string of exclusively Na-sanukitoids (KaSa-NW) lies to the west of the Perseverance Fault, extending from where the Perseverance Fault itself forms the eastern boundary of the Kalgoorlie Terrane, potentially as far northwest to the Agnew region. To the north-northwest of Agnew, additional Na-sanukitoids lying within the Perseverance Fault might also form an extension of KaSa-NW.

To the far north, within the Wiluna greenstone belt, a relatively poorly defined belt of mainly Na-sanukitoids (KaSa-NE) intrudes greenstones between the McClure and Celia Faults. To the east of the Celia Fault, in the Kurnalpi Terrane, a very well-defined northwesterly belt of almost exclusively K-syenites, with minor K-sanukitoids (KuSy-N), extends for around 220 km and sub-parallel the KaSa-NE belt.

## Sanukitoid-like rocks

Sanukitoid-like rocks are so-called because they are mafic granites (mainly diorite to granodioritic) in the sense of Champion and Sheraton (1997) that, like sanukitoid, are generally enriched in large iron lithophile elements (LILE), with  $\text{Sr/Y} > 30$ , but contain less  $\text{MgO}$  (or have a lower  $\text{Mg}^\#$ ), and/or  $\text{Cr}$  and/or  $\text{Ni}$  than is expected through direct derivation from a peridotitic source. In cases where sanukitoid-like rocks and sanukitoids are closely related spatially and temporally, and where compositions are transitional to sanukitoid, sanukitoid-like rocks might legitimately be reclassified as sanukitoid. In our data sets, there are many instances where this might be the case, particularly in the EGST. Thus, the distribution of sanukitoid-like rocks (both Na- and K-) is broadly similar to that of sanukitoids (Fig. 21), with very few occurring in regions where greenstone lithological units are not well represented. In the EGST they define three broadly northwest-trending belts coinciding with sanukitoids and fall along the same western-EGST margin trend defined by  $\text{Na}^+$  and Na High-Ca (high-Sr/Y) granites. Unlike sanukitoids, sanukitoid-like rocks show no clear spatial relationship with syenites, particularly in the EGST. They are virtually absent from the northern and southern Kurnalpi syenite belt.

The compositions of sanukitoid-like rocks is broadly consistent with that expected from primitive members (largely cumulate) of a High-Ca (high-Sr/Y) granite series but whereas the two are commonly spatially related within and near greenstone belts, this is not the case in areas away from greenstones. A more viable suggestion, consistent with the close association with sanukitoids, is that sanukitoid-like rocks form from mantle-derived sanukitoid parental magmas that underwent varying degrees of hybridization with basaltic magmas at the base of the crust. This is also consistent with where the sanukitoid-like rocks plot on an alkalis-iron-magnesium (AFM) (Fig. 16) diagram – between the calc-alkaline field for sanukitoids and tholeiites.

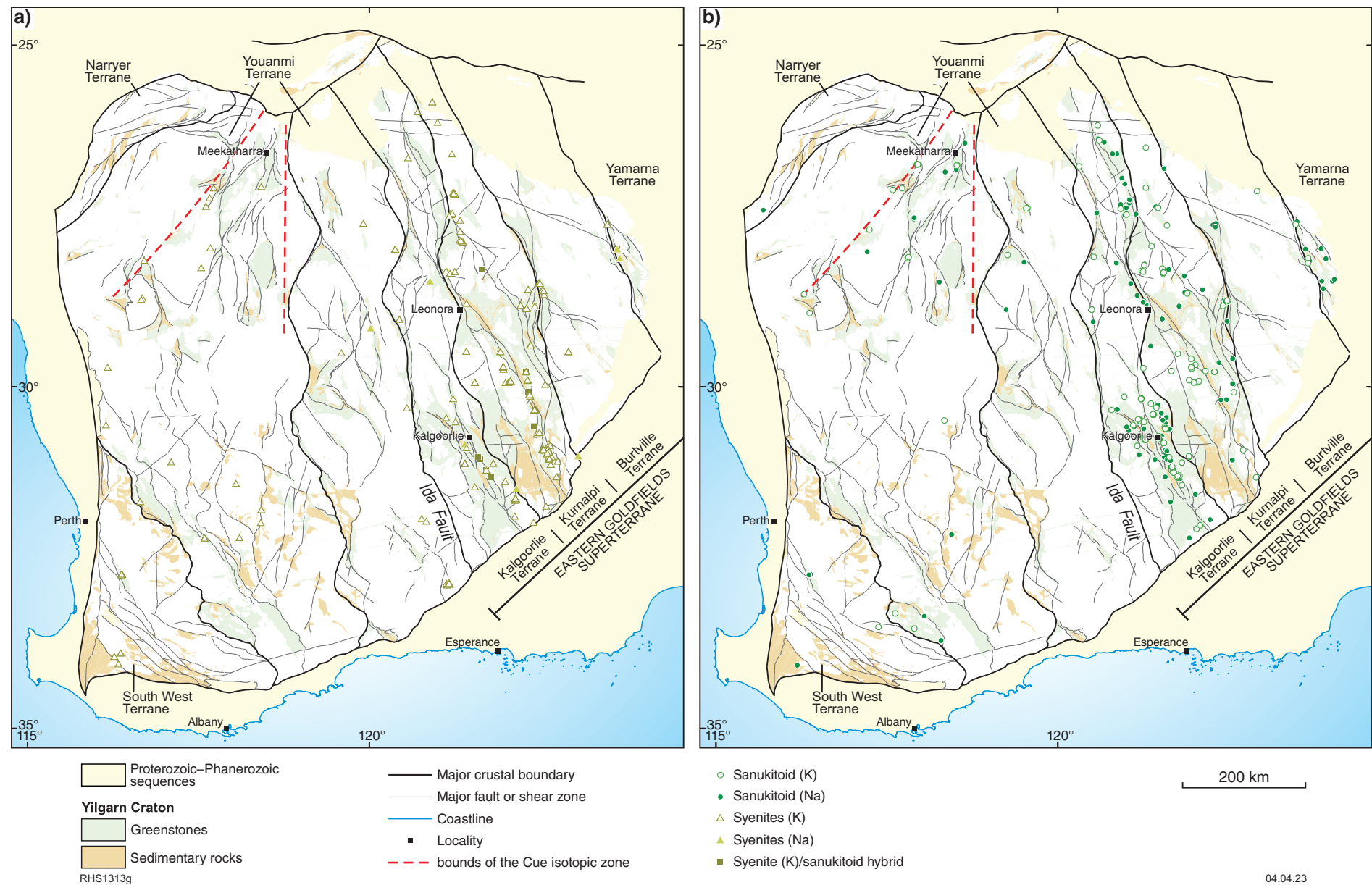


Figure 19. Summarized bedrock geology of the Yilgarn Craton showing the distribution of: a) syenites; b) sanukitoids



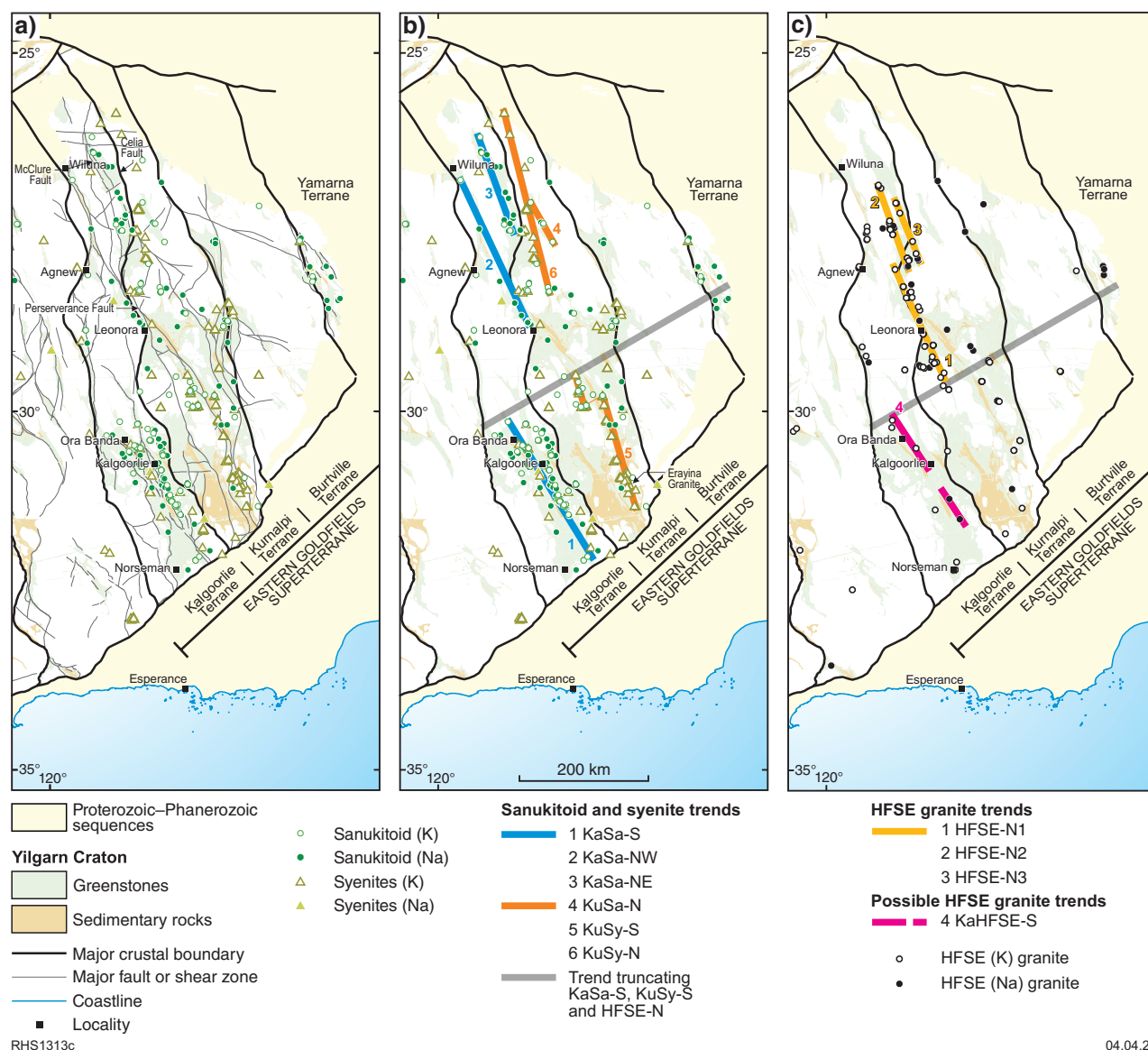


Figure 20. Summarized bedrock geology of the eastern Yilgarn Craton showing: a) the distribution of syenites and sanukitoids; b) the distribution of syenites and sanukitoids and inferred linear distribution trends; c) the distribution of high-HFSE granites and inferred linear distribution trends

## Diorite

Like sanukitoid and sanukitoid-like rocks, these low-Sr/Y dioritic to granodioritic ( $\text{SiO}_2$ , ~57.5 – 70 wt%) mafic granites are concentrated in the greenstone-rich EGST and the Cue isotopic zone of the Youanmi Terrane (Fig. 21). However, they are also found throughout the central Youanmi Terrane and the South West Terrane. Within the EGST, the diorites lie both within and peripherally to the sanukitoid-rich areas and in the northern part of the EGST, lie within a large part of the Leonora HFSE granite belt (HFSE-N1; Fig. 20b).

The diorites cover a wide range of  $\text{Mg}^\#$  at a given silica content and clearly derive from a wide range of parental compositions. Rarer samples with  $\text{Mg}^\#$  as low as 40 at 60 wt%  $\text{SiO}_2$  may reflect examples derived through partial melting of mafic crustal sources. However, whereas most of the diorites would be classified as High-Ca, rather than Low-Ca granites at higher  $\text{SiO}_2$  contents based on (for example) their  $\text{K}_2\text{O}$  vs Ce concentrations, most of the diorites have  $\text{Mg}^\#$  requiring a parental magma of mantle origin.

Hence, unlike High- or Low-Ca granites, most diorites are not dominantly crustal melts. On an AFM diagram (Fig. 16), the diorites span a region that overlaps both the field for calc-alkaline sanukitoids and the field for evolved tholeiites. Compared to sanukitoids and sanukitoid-like rocks, the mantle-normalized trace element patterns for diorites are very similar to those of High-Ca (low-Sr/Y) granites, showing flatter HREE patterns at higher element concentrations as well as significant negative Sr anomalies – suggestive, in the case of diorites, of hotter and drier parental magmas formed from either less enriched or shallower mantle sources.

A rarer group of diorites would be classified as Low-Ca granites at higher  $\text{SiO}_2$  contents based on (for example) their  $\text{K}_2\text{O}$  vs Ce concentrations. These occur mainly in the South West Terrane and in the southwestern Youanmi Terrane, commonly associated with Low-Ca granites, and typically contain abundant biotite-rich schieren, in places ranging to diatextitic migmatite. In contrast with other diorites, these Low-Ca diorites likely do reflect crustal melts.



RHS1313n

13.01.23

Figure 21. Summarized bedrock geology of the Yilgarn Craton showing the distribution of sanukitoid, sanukitoid-like rocks and diorite

At the craton scale, available dating suggests that diorite magmatism accompanies all major periods of High-Ca (high- and low-Sr/Y) magmatism (Fig. 17). Records of diorite magmatism between c. 3007 and c. 2941 Ma are preserved primarily in the northwest Youanmi Terrane (Fig. 6), with a slightly longer age range (3023–2925 Ma) for High-Ca (high-Sr/Y) magmatism and a shorter and younger age range for High-Ca (low-Sr/Y) magmatism (2939–2921 Ma). All three magma groups are represented in the northern Youanmi Terrane between c. 2810 and c. 2760 Ma and again, along with the northeastern part of the EGST (Burtville and Yamarna Terranes), between c. 2770 and c. 2715 Ma.

Relatively few age data are available from diorites in the EGST. Here, diorite, High-Ca (high- and low-Sr/Y) granite, sanukitoid and sanukitoid-like magmatism all commenced at c. 2703 Ma and while diorite magmatism appears to have essentially stopped by c. 2674 Ma, High-Ca magmatism continues to c. 2650 Ma and sanukitoid magmatism continues to c. 2644 Ma.

## Significance of regional- and craton-scale trends

The Yilgarn Craton is traditionally subdivided into northerly trending tectonic ‘terrane’ interpreted to reflect an exotic origin, based on demonstrated or inferred geological differences. Such inferences might be more robust for some terranes (e.g. the Narryer Terrane), but not for others. Indeed, rather than invoking terrane accretion processes, many recent models consider the EGST to reflect a magma-dominated rift overlying continuous Youanmi Terrane basement (e.g. Pawley et al., 2012; Smithies et al., 2018b; Mole et al., 2019).

We use the distributions in granite types, as discussed above, to infer variations in source compositions, melting conditions and modes of emplacement that might help place constraints on the evolution of the Yilgarn Craton. Many of the geochemical patterns we observe are in accord with those identified by Champion and Cassidy (2007), Champion and Cassidy (2013) and Mole et al. (2019) through isotopic mapping of the Yilgarn Craton, although with some modifications.

## Regional granite domains

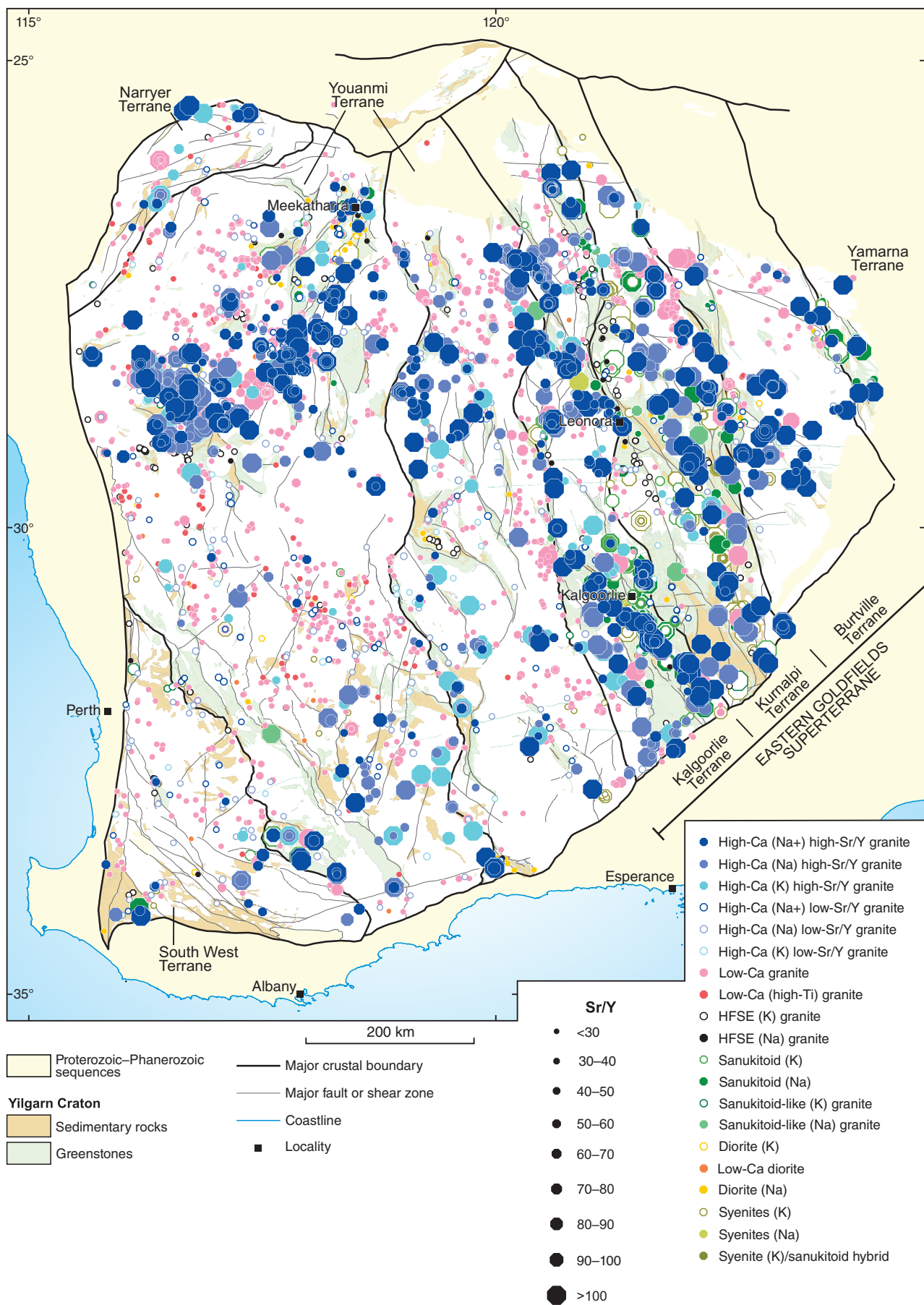
One of the most intriguing associations is the clear increase in granite compositional diversity in proximity to greenstone belts. This is best exemplified by the close association of high-Sr/Y granites, particularly Na<sup>+</sup> and Na High-Ca (high-Sr/Y) granites, and sanukitoids with greenstones. Hence, at the craton scale, the distribution of Na<sup>+</sup> (and Na) High-Ca (high-Sr/Y) granites is mainly concentrated in or near greenstone belts in the northern half of the craton (northern Youanmi Terrane high-Sr/Y granite zone), and an east-northeasterly trending domain along the southeastern part of the craton (southern Youanmi Terrane high-Sr/Y granite zone) and in the EGST. The higher Sr/Y representatives of other granites types, including Low-Ca granites, also tend

to fall in these zones. Indeed, plotting the entire database (all granite types) in terms of Sr/Y still identifies the central Youanmi Terrane to have a fundamentally low abundance of low-Sr/Y granites (Fig. 22). This spatial variation could be interpreted as reflecting a central Youanmi Terrane region where crustal melting occurred at lower pressures (<0.7 GPa where plagioclase was stable but garnet was not stable, e.g. Champion and Smithies, 2007; Johnson et al., 2017) flanked to the north and southeast by zones where melting occurred at higher pressures and/or was of a more LILE-enriched source (Smithies et al., 2009; Moyan and Martin, 2012; Johnson et al., 2017). A further, and likely related, general observation is that High-Ca (low-Sr/Y) granites and Low-Ca granites tend to be more commonly associated with the large granite-dominated regions peripheral to, or distal from, greenstone belts than do High-Ca (high-Sr/Y) granites. In the northern and southern Youanmi Terrane high-Sr/Y granite zone and in the EGST, the association of high-Sr/Y granites, particularly Na<sup>+</sup> and Na High-Ca (high-Sr/Y) granites and sanukitoids, with greenstones, highlights a potentially fundamental point – that greenstone-forming processes and melting of crustal sources that are deep and/or LILE-enriched or of mantle lithospheric sources, are strongly linked. A corollary of this might be that areas lacking, or with very few, high-Sr/Y felsic rocks, such as the central Youanmi Terrane, might never have underlain significant tracts of greenstones. Conversely, those areas apparently distal from greenstones but with a high granite diversity, particularly if this includes high-Sr/Y granites, sanukitoids, syenites or diorites, might reflect the root zones to eroded greenstones.

On balance, the features described above imply a fundamental difference between the southern and northern Youanmi Terrane high-Sr/Y granite zones and the central Youanmi Terrane in either the bulk source of granites or the depth of crustal melting, or both. Given the strong association between greenstones and high-Sr/Y granites, these differences might somehow be linked to the formation, or abundance, of upper crustal greenstone belts. The most obvious relationship would be that the mantle heat input associated with channelling mafic magmas along major structures to form greenstone belts also resulted in deep crustal melting forming high-Sr/Y magmatism. Regardless, the boundaries between the southern and northern Youanmi Terrane high-Sr/Y granite zones and the central Youanmi Terrane strike almost at right angles to the dominant north-northwest structural trend of the craton and its terranes, including the Youanmi Terrane/EGST boundary, and pre-date them.

Further east, in the EGST, the northern parts of both the southern sanukitoid and syenite trends – KaSa-S and KuSy-S – and the southern part of the major north-northeasterly HFSE trend – HFSE-N1 – all truncate along a broadly east-northeast trend (Fig. 20c). This also coincides with a series of sharp gradients in the regional contoured Nd- and Hf-isotope maps of the EGST, including a very significant apparent offset, or embayment, in the contoured data to the north of Kalgoorlie (Fig. 23). Additionally, these features also coincide with what would be an eastward extrapolation of the northern margin of the southern Youanmi Terrane high-Sr/Y granite zone (Fig. 23).





RHS1318a

13.02.23

Figure 22. Summarized bedrock geology of the Yilgarn Craton showing all granite data with symbol size scaled to Sr/Y ratio

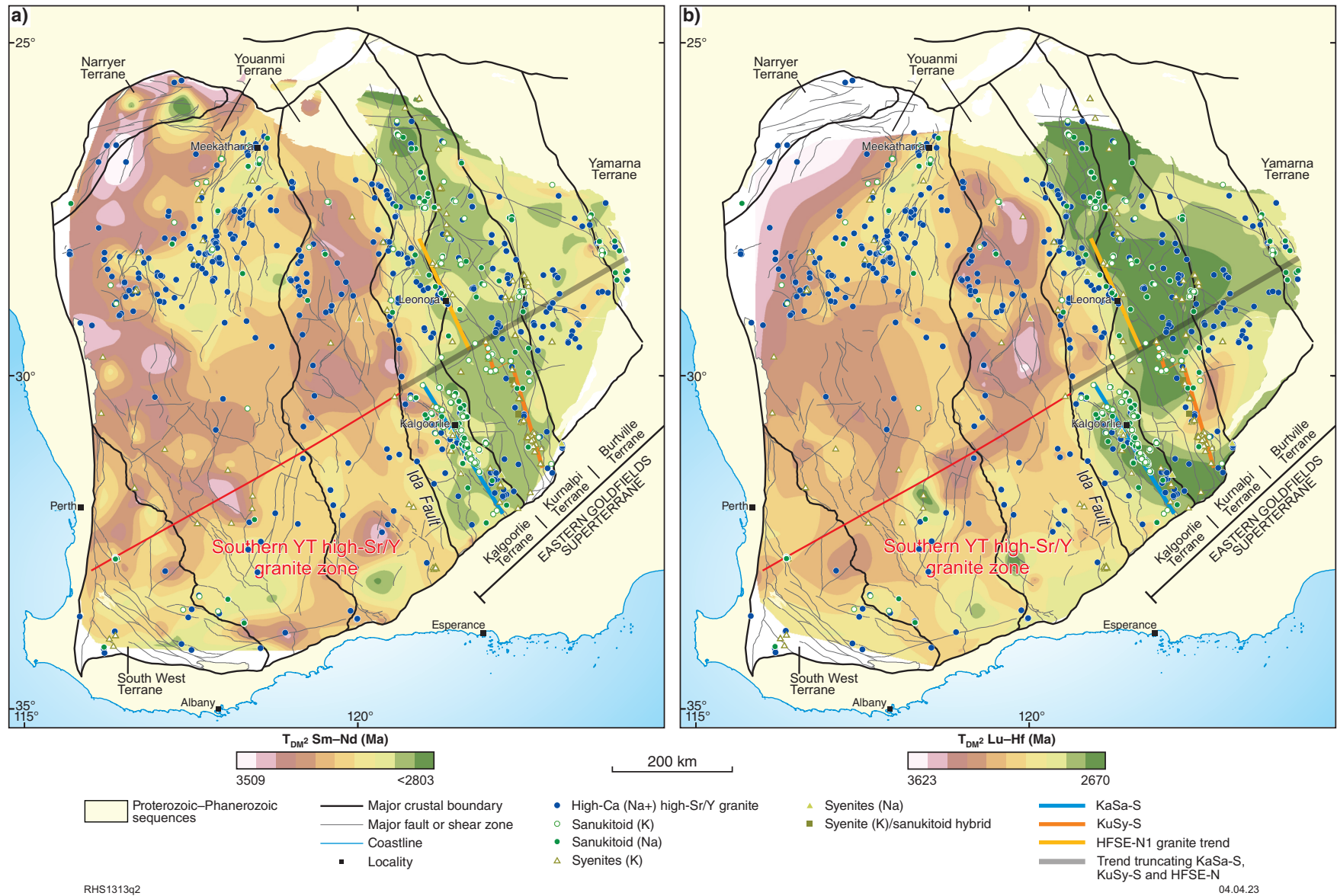


Figure 23. Regional outline of the Yilgarn Craton overlaying the distribution of High-Ca, high-Sr/Y granites, sanukitoids and syenites on contour maps showing variations in model ages ( $T_{DM}^2$ ) from: a) Sm-Nd isotope measurements; b) Lu-Hf isotope measurements; also showing the northern boundary of the Southern YT high-Sr/Y granite zone (isotope data from Lu et al., 2021a,b)

## Young juvenile crustal additions

Several iterations of regional contoured Nd- and Hf-isotope maps of the Yilgarn Craton are available (Champion and Cassidy, 2007, 2013; Mole et al., 2019; Lu et al., 2021a; Lu et al., 2021b). Some versions of these maps are constructed specifically excluding felsic rocks with a significant suspected, direct, mantle source component (e.g. Champion and Cassidy, 2007, 2013, which mainly plot data from High- and Low-Ca granites), whereas others have included all felsic units irrespective of interpreted source (e.g. Lu et al., 2021a,b). Irrespective, all of these maps show a sharp gradient between the radiogenic felsic upper crust of the western EGST and the relatively non-radiogenic felsic upper crust of the Youanmi Terrane (Fig. 24). This gradient remains one of the foundations of east–west terrane accretion paradigms for the c. 2.7 Ga evolution of the Yilgarn Craton. Although the sharp gradient locally shows poor correlation with the Ida Fault, which is believed to be the structural expression of the terrane boundary, it might be argued that this reflects the eastward dip of a Youanmi slab and/or post-accretion realignment of the putative suture. Nevertheless, embayments of non-radiogenic felsic crust contiguous with the Youanmi Terrane extend eastwards across the Ida Fault for up to 80 km. Other zones of less radiogenic crust also occur throughout the EGST.

Figure 24 compares regional Nd-isotope maps that contour various datasets, including: data from all granitic rock groups (following Lu et al., 2021a,b) (Fig. 24a); data exclusively from High- and Low-Ca granites (following Champion and Cassidy, 2007, 2013) (Fig. 24b); data from High- and Low-Ca granites within crystallization ages between 3640 and 2710 Ma (Fig. 24c); and data from High- and Low-Ca granites within crystallization ages between 2710 and 2600 Ma samples (Fig. 24d). The c. 2710 Ma age broadly corresponds to the stratigraphic base of greenstone sequences that characterize much of the EGST, although no mafic units directly contribute to the isotopic data.

Although relatively few Nd-isotope data exist for the 3640 and 2710 Ma time slice (Fig. 24c), the regional pattern is perhaps consistent with a gradual easterly or southeasterly decrease in age of crustal sources of granite magmas. What is absent from the dataset is any evidence that any of the major terrane boundary faults separate isotopically exotic crust. The implication here is that the isotopically juvenile material we now see to the west of the Ida Fault was added to the crust after c. 2710 Ma.

After c. 2710 Ma, the isotopic pattern of the western Yilgarn Craton (Youanmi Terrane) changes very little (c.f. Fig. 24a,c). However, to the east of the Ida Fault, it is clear that the abundance of lithospheric mantle-derived magmas – sanukitoids, HFSE granites, syenites, and probably some of the Na+ High-Ca (high-Sr/Y) granites – significantly influences the juvenile isotopic map patterns (Fig. 24a). However, this pattern is not entirely dependent on analyses of magmas with a mantle source component since many of the crustal-derived rocks within the 2710 and 2600 Ma time slice – High-Ca (low-Sr/Y) granites and Low-Ca granites – in the EGST also have more radiogenic Nd and Hf compositions (e.g. Fig. 14 and c.f. Fig. 24a,b) than otherwise compositionally similar samples of similar age from the Youanmi Terrane. This, however, is mainly restricted

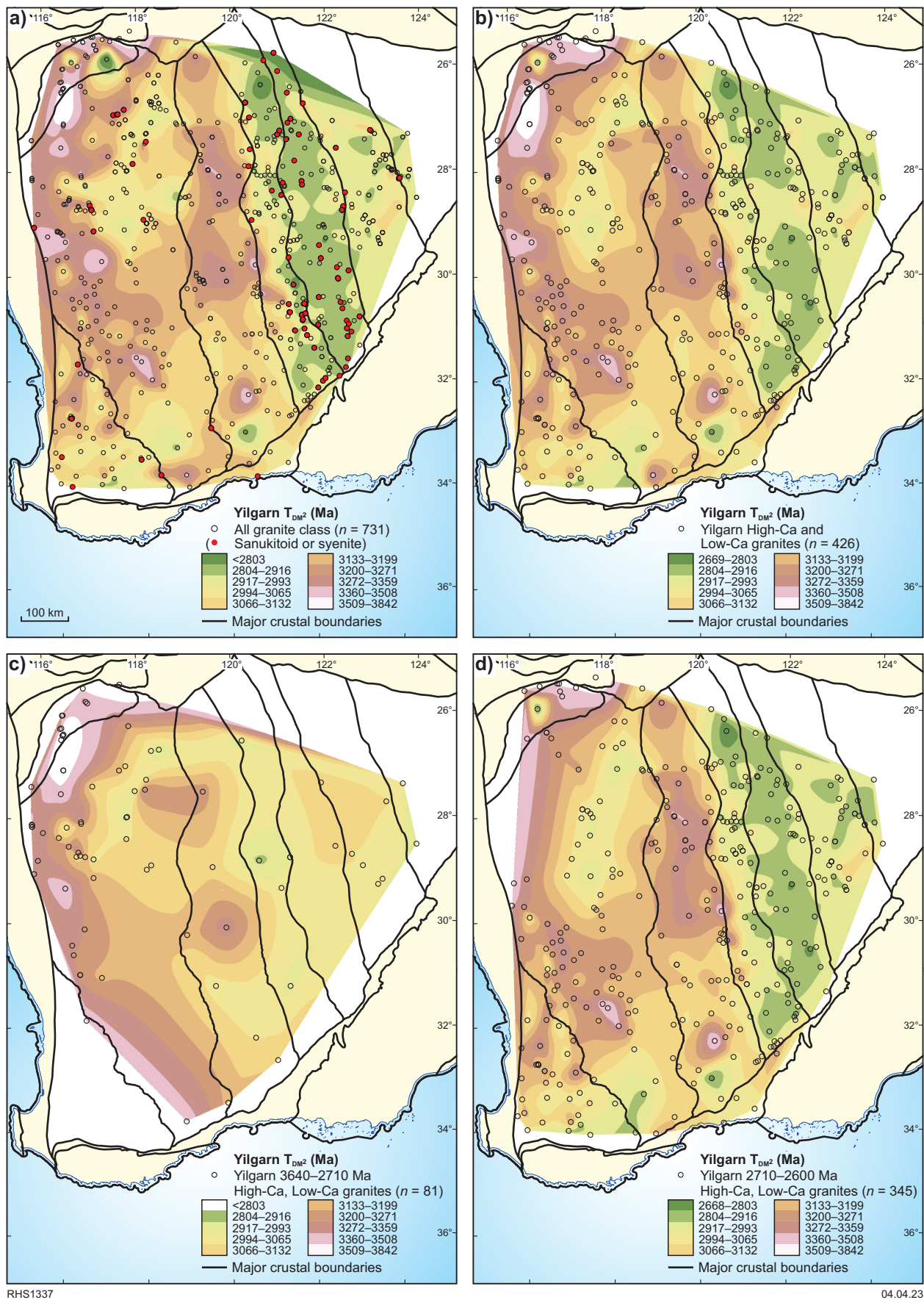
to samples close to greenstones rich in sanukitoids and syenites and suggests that the source to those anomalously radiogenic crustal melts actually included lower crustal equivalents of the sanukitoid and syenites emplaced at or shortly before partial melting of the crust.

Thus, the presence and distribution of the radiogenic felsic upper crust throughout the EGST reflects the variable isotopic overprint, on Youanmi Terrane-like crust, of juvenile, mantle-derived mafic and felsic magmas. A similar argument is clearly applicable to the relatively radiogenic crust of the Cue isotopic zone. This presence of particularly radiogenic ‘juvenile’ crust distinguishes the EGST from much of the Youanmi Terrane but was a feature acquired only late in the magmatotectonic evolution of the Yilgarn Craton and of the EGST. It is not necessarily a reflection of, or evidence for, the juxtaposition of intrinsically distinct crustal blocks, but simply of a process that channelled mantle-derived melts into the crust. These conclusions question the idea that the north-northwest tectonic grain of the EGST directly relates to some form of east–west terrain accretionary tectonic process.

The present distribution of embayments in the isotopic map across the Ida Fault may have several explanations. These include actual block displacement (faulting) along, in the present case, broadly east-northeasterly striking structures, perhaps propagating along old basement structures such as the one potentially identified by the southern Youanmi Terrane high-Sr/Y granite zone boundary. If this explanation is valid then much of the physical evidence in terms of clear mappable offsets of greenstones must have been largely obscured by subsequent magmatism and transpressional displacement within the north-northeast fault network of the EGST.

The alignment of the northern edge of the southern Youanmi Terrane high-Sr/Y granite zone with one of the major embayments in the isotopic map and with the terminations of the KaSa-S, KuSy-S and HFSE-N1 trends (Fig. 23) invites the suggestion that the locations of the embayments and the location of the KaSa-S, KuSy-S and HFSE-N1 trends was influenced by a pre-existing basement anisotropy – the extension of the southern Youanmi Terrane high-Sr/Y granite zone basement beneath the EGST. Hence, an alternative explanation for the observed embayments in the isotopic map is that the distribution of inputs of sanukitoid and syenite was controlled by the interaction of broadly east-northeasterly striking basement structures with the array of north-northwesterly striking translithospheric fractures that now dominate the overprinted structural grain of the EGST to allow northwest-trending sanukitoid-syenite zones. This may have occurred near the end of the main mafic magmatic period that produced the broadly 2715 to 2692 Ma components of the Kalgoorlie Group (Hannans Subgroup). However, the very strong spatial association of sanukitoids with greenstone belts suggests these northwest-trending zones were the same primary basin-forming features along which those mafic and ultramafic magmas were earlier channelled. The implication here is that greenstone formation is a necessary step in forming the hydrated mantle sources required to form sanukitoids and possibly also syenites.





RHS1337

04.04.23

Figure 24. Regional outline of the Yilgarn Craton comparing Nd-isotope contour maps utilizing various datasets: a) data from all granitic rock groups (following Lu et al., 2021a,b); b) data exclusively from High- and Low-Ca granites (following Champion and Cassidy, 2007, 2013); c) data from High- and Low-Ca granites with crystallization ages between 3640 and 2710 Ma; d) data from High- and Low-Ca granites with crystallization ages between 2710 and 2600 Ma

## Other patterns

Our new granite compilation includes several other examples where regional linear granite compositional boundaries do not coincide with mapped surface traces of inferred crustal-scale faults. The most obvious case involves the Ida Fault, discussed above, which is regarded as separating the Kalgoorlie Terrane (EGST) from the Youanmi Terrane. This structure is more confidently identified both in field observations and seismic interpretations in the north of the craton than in the south, although it is unclear as to whether it, or a subsidiary structure – the Waroonga Shear Zone – marks the actual northern terrane junction. A map showing Na+ and Na High-Ca (high-Sr/Y) granites and Low-Ca granites (Fig. 10) shows a regional boundary, paralleling the presently recognized position of the Ida Fault. Although the data coverage is poor in some critical areas, the granite distribution patterns do not appear to coincide with the Ida Fault, but rather to broadly align, from north to south, with the Waroonga Shear Zone, Ballard Fault, Kunanaling Shear Zone and the Bullabulling Shear Zone.

Our data also identify a northwest-trending belt of Low-Ca (high-Ti) granites associated with abundant Low-Ca granites, in the western marginal zone of the Youanmi Terrane and extending up to 200 km into the Youanmi Terrane (Fig. 11). This belt of granites closely matches the distribution of older basement components as inferred from Hf- and Nd-isotope maps (Fig. 23). The belt of Low-Ca (high-Ti) granites does not appear to extend into the southern Youanmi Terrane high-Sr/Y granite zones, perhaps strengthening the suggestion of a fundamental crustal-scale difference between that zone and the central Youanmi Terrane crust.

The distribution of the 3010–2920 Ma Southern Cross Supergroup and Thundelarra Supersuite in parts of the Youanmi Terrane with older Nd model ages led to the idea of a proto-Yilgarn Craton at c. 2.9 Ga (Ivanic et al., 2022). This horseshoe-shaped distribution of older basement and older greenstones and older granitic magmatism coincides with the increase in Low-Ca and Low-Ca (high-Ti) granitic rocks (Fig. 2).

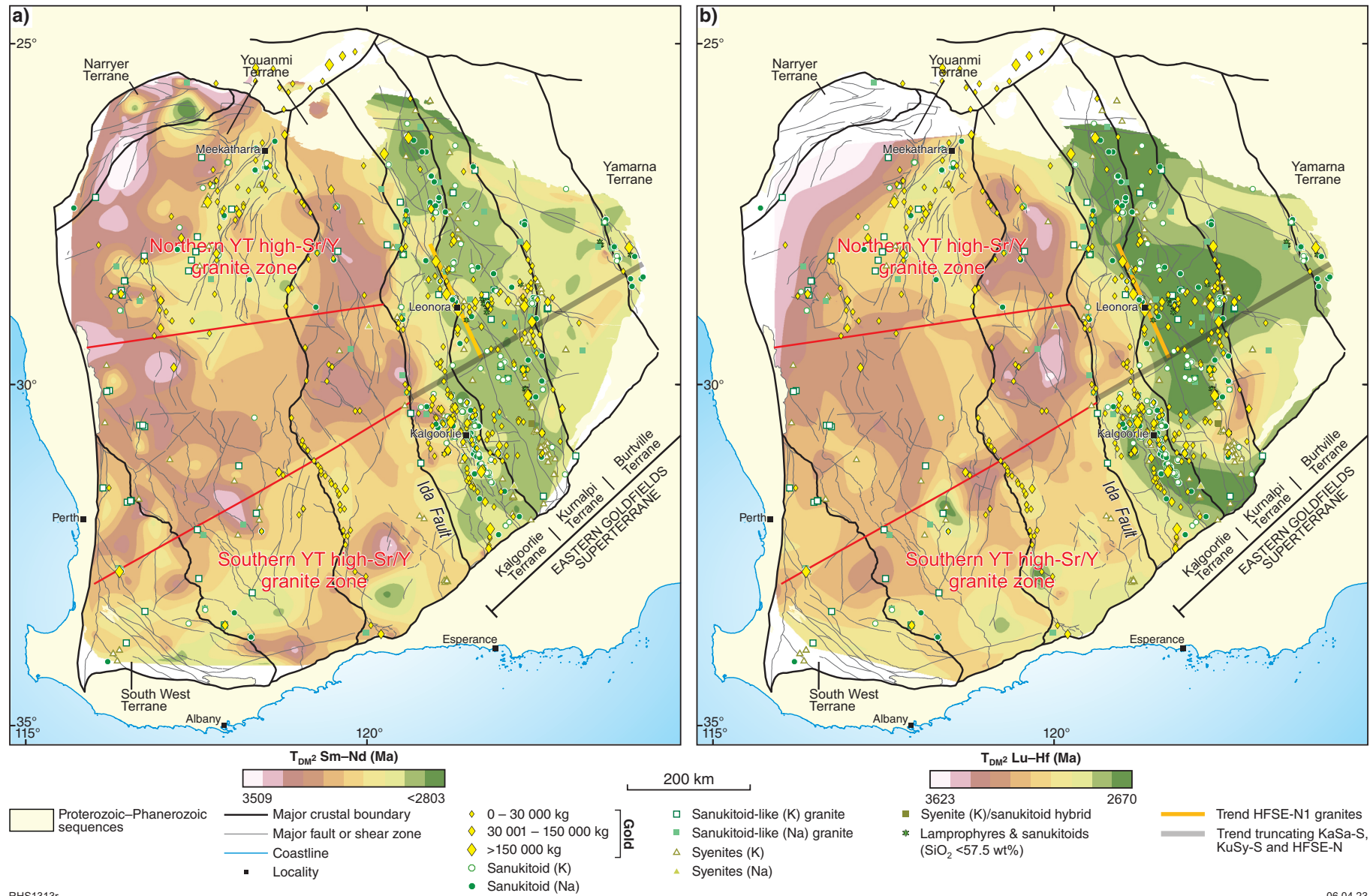
If the presence of Low-Ca (high-Ti) granites does reflect melting at higher temperature than those normally required to form Low-Ca granites, then one explanation for the presence of the Low-Ca (high-Ti) granite zone along the Youanmi Terrane boundary is that lower crust in this region still contained fusible material at temperatures above where other sources were already melt depleted. This material was likely a component of the older crustal material that was already refractory through partial reworking during a previous thermal event. Irrespective, the Low-Ca (high-Ti) granite zone almost certainly represents a significant crustal architectural feature. Interestingly, the observation that Low-Ca granites have higher average emplacement temperatures than the High-Ca granites and sanukitoids, are mainly younger than those granites and the greenstones, show no clear spatial association with greenstone, and have magmatic temperatures of emplacement that increase with decreasing emplacement age, suggests that the mantle was not the main source of heat required to melt the source of the Low-Ca granites.

## Granites, greenstones and gold

A strong spatial and temporal association between sanukitoids and/or syenites and gold mineralization in the EGST has already been noted (e.g. Champion and Cassidy, 1998; Witt et al., 2013, 2015; Smithies et al., 2018c). According to Witt et al. (2013), one of the strongest statistical associations with gold mineralization in the Kalgoorlie and Kurnalpi Terranes is achieved by combining all intrusions with a metasomatized mantle source component, which resulted in capture of 54.1% of the gold endowment and 19.4% of deposits in the 1-km buffer of the intrusions. The accuracy of this estimate depends significantly on the number of felsic samples that are submitted for complete whole rock geochemical analysis and properly classified and reported. Based on our data, we would suggest that the distribution and volume of sanukitoids and syenites has previously been grossly underestimated, particularly given the extent of radiogenic crust in the EGST (Fig. 25). These observations do not deny the often important role that 'orogenic' (re)mobilization of gold likely played in producing economic gold deposits (e.g. Fayol and Jébrak, 2017).

Viewing estimates of Au-endowment (resource estimate plus production data) of existing Au mines together with the locations of known sanukitoids and syenite (Fig. 25) it appears that gold mineralization in general, and large gold deposits in particular, are extremely rare in areas of relatively old crust (e.g. Cassidy and Champion, 2004) or in areas of low granite diversity. Such areas are widespread throughout the Youanmi Terrane. They are characterized by a lack of sanukitoid magmatism and a large apparent gap between the average age of greenstone formation and the apparent ( $T_{DM}^2$  model age) age of basement – itself strongly influenced by the presence, or otherwise, of sanukitoid magmatism, based on relationships in the EGST. The most notable exception is in the case of the Cue isotopic zone, which is locally well endowed with gold mineralization and spatially associated sanukitoid and syenite magmatism. It is possible, in this respect, that the small age difference between greenstone formation and apparent basement  $T_{DM}^2$  values reflects a useful regional indicator of gold prospectively.

Conversely, the area of greatest gold endowment (the Kalgoorlie–Kambalda region) also appears to be the area with the largest concentration of sanukitoids, although this observation is clearly open to sampling bias in this particularly well-studied region. Nevertheless, throughout the EGST, there are numerous regions where sanukitoids (and syenites) have been sampled or are common, but where significant gold mineralization has not yet been detected – or, where radiogenic crust is known to underlie greenstone belts where neither sanukitoids (or syenites) nor gold mineralization have yet to be detected. However, more comprehensive Nd- and Hf-isotopic datasets are required to refine these relationships.



RHS1313r

06.04.23

Figure 25. Regional outline of the Yilgarn Craton overlaying the distribution of sanukitoids and syenites and of gold deposits on contour maps showing variations in model ages ( $T_{DM}^2$ ) from: a) Sm-Nd isotope measurements; b) Lu-Hf isotope measurements (isotope data from Lu et al., 2021a,b)



## Conclusions

Applying a systematic geochemical classification to a large dataset of high-quality geochemical analyses of felsic rocks from the Archean Yilgarn Craton allows the meaningful interrogation of spatial relationships within and between various lithochemical granites groups. Such relationships or trends are controlled by variations in bulk source compositions and by melting conditions, and reflect variations in lithosphere-scale crustal architecture. Our preliminary analysis of the presently available data clearly identifies the influence that major, known, visible, structural features have had on controlling the emplacement of felsic magmas. However, they also identify regions – commonly broadly linear – that most likely reflect an older, cryptic basement architecture. A pre-3000 Ma refractory source component is inferred in the crustal source region to some Low-Ca granites of the Youanmi Terrane. In contrast, easterly, or northeasterly trending sources produce regions of high-Sr/Y, and generally sodic, granites in the northern and southern parts of the craton. The distribution of granites that include a significant direct mantle source component is well constrained by major northwest-striking structures and by proximity to northwest-striking greenstone belts and in the case of sanukitoids, strongly correlates with the occurrence of gold mineralization. Even though this primitive (mantle) contribution represents a very late addition to the crustal evolution of the Yilgarn Craton, its distribution appears to have been influenced by older basement heterogeneities.

## References

- Cassidy, KF and Champion, DC 2004, Crustal evolution of the Yilgarn Craton from Nd isotopes and granite geochronology: Implications for metallogeny, *in* Extended Abstracts edited by JR Muhling, R Goldfarb, N Vielreicher, FP Bierlein, E Stumpf, DI Groves, S Kenworthy and CM Knox-Robinson: SEG 2004, Predictive Mineral Discovery Under Cover, Perth, Western Australia, 2004/09/27: Centre for Global Metallogeny, The University of Western Australia, p. 317–320.
- Cassidy, KF, Champion, DC, Krapež, B, Barley, ME, Brown, SJA, Blewett, RS, Groenewald, PB and Tyler, IM 2006, A revised geological framework for the Yilgarn Craton, Western Australia: Geological Survey of Western Australia, Record 2006/8, 8p.
- Champion, DC and Cassidy, KF 1998, Metallogenic potential of granitoids: Kanowna Belle and Granny Smith regions: Final report to Golden Valley Joint Venture and Placer Pacific Ltd., Australian Geological Survey Organisation (unpublished).
- Champion, DC and Cassidy, KF 2002, Chapter 2. Granites of the northern Eastern Goldfields: their distribution, age, geochemistry, petrogenesis, relationship with mineralisation, and implications for tectonic environment, *in* The characterisation and metallogenic significance of Archean granitoids of the Yilgarn Craton, Western Australia edited by KF Cassidy, DC Champion, NJ McNaughton, IR Fletcher, AJ Whitaker, IV Bastrakova and A Budd: Minerals and Energy Research Institute of Western Australia, MERIWA Project no. M281/AMIRA Project no. 482 (Report No. 222), 2.1–2.49 + 14 figures.
- Champion, DC and Cassidy, KF 2007, An overview of the Yilgarn and its crustal evolution, *in* Proceedings of Geoconferences (WA) Inc. Kalgoorlie '07 Conference, 26–27 September, Kalgoorlie, Western Australia edited by FP Bierlein and CM Knox-Robinson: Geoscience Australia, Record 2007/14, p. 8–13.
- Champion, DC and Cassidy, KF 2013, Geodynamics: using geochemistry and isotopic signatures of granites to aid mineral systems studies: an example from the Yilgarn Craton: Geoscience Australia, Record 2008–2009, p. 7–16.
- Champion, DC and Sheraton, JW 1997, Geochemistry and Nd isotope systematics of Archean granites of the Eastern Goldfields, Yilgarn Craton, Australia: implications for crustal growth processes: Precambrian Research, v. 83, no. 1–3, p. 109–132, doi:10.1016/S0301-9268(97)00007-7.
- Champion, DC and Smithies, RH 2007, Geochemistry of Paleoarchean granites of the East Pilbara Terrane, Pilbara Craton, Western Australia: implications for early Archean crustal growth, *in* Earth's oldest rocks edited by MJ Van Kranendonk, VC Bennett and RH Smithies: Elsevier B.V., Burlington, Massachusetts, USA, Developments in Precambrian Geology 15, p. 369–410.
- Cox, K, Bell, J and Pankhurst, R 1979, The interpretation of igneous rocks: Springer, London.
- Czarnota, K, Champion, DC, Cassidy, KF, Goscombe, B, Blewett, R, Henson, PA and Groenewald, PB 2010, Geodynamics of the eastern Yilgarn Craton: Precambrian Research, v. 183, p. 175–202.
- Fayol, N and Jébrak, M 2017, Archean sanukitoid gold porphyry deposits: a new understanding and genetic model from the Lac Bachelor Gold Deposit, Abitibi, Canada: Economic Geology, vol. 112, p. 1913–1936.
- Geological Survey of Western Australia 2022, West Yilgarn, 2022: Geological Survey of Western Australia, Geological Information Series.
- Ivanic, TJ, Wingate, MTD, Lowrey, JR and Lu, Y 2022, Formation of the Yilgarn protocraton by rift-related magmatism from 3.01 to 2.92 Ga: Geological Survey of Western Australia, Report 232, 34p.
- Johnson, TE, Brown, M, Gardiner, NJ, Kirkland, CL and Smithies, RH 2017, Earth's first stable continents did not form by subduction: Nature, v. 543, no. 7644, p. 239–242.
- Kuno, H 1968, Differentiation of basalt magmas, *in* The Poldervaart treatise on rocks of basaltic composition edited by HH Hess: Interscience, New York.
- Lowrey, JR and Smithies, RH 2022, Eastern Goldfields geochemical barcoding project – notes to accompany 2022 data release: Geological Survey of Western Australia, Record 2022/8.
- Lowrey, JR, Smithies, RH and Champion, DC 2022, Yilgarn granite project – notes to accompany 2022 data release: Geological Survey of Western Australia, Record 2022/9, 3p.
- Lowrey, JR, Smithies, RH, Champion, DC and Cassidy, KF 2023, Systematic classification of Yilgarn Craton granitic rocks: Geological Survey of Western Australia, Record 2023/12.
- Lu, Y, Wingate, MTD, Champion, DC, Smithies, RH, Johnson, SP, Mole, DR, Poujol, M, Zhao, J, Maas, R and Creaser, RA 2021a, Samarium–neodymium isotope map of Western Australia, *in* Accelerated Geoscience Program extended abstracts compiled by Geological Survey of Western Australia: Geological Survey of Western Australia Record 2021/4, p. 10–12.
- Lu, Y, Wingate, MTD, Romano, SS, Mole, Kirkland, CL, Kemp, AIS, Belousova, EA, Smithies, RH, Gessner, K and Johnson, SP 2021b, Zircon lutetium–hafnium isotope map of Western Australia: Geological Survey of Western Australia; data layer, <www.dmirs.wa.gov.au/geoview>.
- Martin, H, Smithies, RH, Rapp, R, Moyen, J-F and Champion, DC 2005, An overview of adakite, tonalite–trondhjemite–granodiorite (TTG), and sanukitoid: relationships and some implications for crustal evolution: Lithos, v. 79, p. 1–24, doi:10.1016/j.lithos.2004.04.048.
- Mole, DR, Kirkland, CL, Fiorentini, ML, Barnes, SJ, Cassidy, KF, Isaac, C, Belousova, EA, Hartnady, M and Thebaud, N 2019, Time-space evolution of an Archean craton: A Hf-isotope window into continent formation: Earth-Science Reviews, v. 196, p. 102831, doi:10.1016/j.earscirev.2019.04.003.
- Moyen, J-F and Martin, H 2012, Forty years of TTG research: Lithos, v. 148, p. 312–336, doi:10.1016/j.lithos.2012.06.010.
- Pawley, MJ, Wingate, MTD, Kirkland, CL, Wyche, S, Hall, CE, Romano, SS and Doublier, MP 2012, Adding pieces to the puzzle: Episodic crustal growth and a new terrane in the northeast Yilgarn Craton, Western Australia: Australian Journal of Earth Sciences, v. 59, no. 5, p. 603–623, doi:10.1080/08120099.2012.696555.

- Perring, CS, Barley, ME, Cassidy, KF, Groves, DI, McNaughton, NJ, Rock, NMS, Bettenay, LF, Golding, SD and Hallberg, JA 1989, The association of linear orogenic belts, mantle-crustal magmatism, and Archean gold mineralization in the Eastern Yilgarn Block of Western Australia, *in* The Geology of Gold Deposits: The Perspective in 1988 *edited by* RR Keays, WRH Ramsay and DI Groves: Economic Geology, Monograph 6, p. 571–584.
- Quentin de Gromard, R, Ivanic, TJ and Zibra, I 2021, Pre-Mesozoic interpreted bedrock geology of the southwest Yilgarn, 2021, *in* Accelerated Geoscience Program extended abstracts *compiled by* Geological Survey of Western Australia: Geological Survey of Western Australia Record 2021/4, p. 122–144.
- Shand, SJ 1922, The problem of the alkaline rocks: Proceedings of the Geological Society of South Africa, v. 25, p. xix–xxxiii.
- Shirey, SB and Hanson, GN 1984, Mantle-derived Archean monzodiorites and trachyandesites: *Nature*, v. 310, p. 222–224.
- Smithies, RH, Champion, DC and Van Kranendonk, MJ 2009, Formation of Paleoproterozoic continental crust through intracrustal melting of enriched basalt: *Earth and Planetary Science Letters*, v. 281, no. 3, p. 298–306.
- Smithies, RH, Lu, Y, Gessner, K, Wingate, MTD and Champion, DC 2018a, Geochemistry of Archean granitic rocks in the South West Terrane of the Yilgarn Craton: Geological Survey of Western Australia, Record 2018/10, 13p.
- Smithies, RH, Ivanic, TJ, Lowrey, JR, Morris, PA, Barnes, SJ, Wyche, S and Lu, Y-J 2018b, Two distinct origins for Archean greenstone belts: *Earth and Planetary Science Letters*, v. 487, p. 106–116.
- Smithies, RH, Lu, Y, Johnson, TE, Kirkland, CL, Cassidy, KF, Champion, DC, Mole, DR, Zibra, I, Gessner, K, Sapkota, J, De Paoli, MC and Pujol, M 2019, No evidence for high-pressure melting of Earth's crust in the Archean: *Nature Communications*, v. 10, article no. 5559.
- Smithies, RH, Lu, Y, Kirkland, CL, Cassidy, KF, Champion, DC, Sapkota, J, De Paoli, MC and Burley, L 2018c, A new look at lamprophyres and sanukitoids, and their relationship to the Black Flag Group and gold prospectivity: Geological Survey of Western Australia, Record 2018/15, 23p.
- Stern, RA, Hanson, GN and Shirey, SB 1989, Petrogenesis of mantle-derived, LILE-enriched Archean monzodiorites and trachyandesites (sanukitoids) in southwestern Superior Province: *Canadian Journal of Earth Sciences*, v. 26, p. 1688–1712.
- Watson, EB and Harrison, TM 1983, Zircon saturation revisited: Temperature and composition effects in a variety of crustal magma types: *Earth and Planetary Science Letters*, v. 64, no. 2, p. 295–304.
- Witt, WK, Ford, A and Hanrahan, B 2015, District-scale targeting for gold in the Yilgarn Craton: Part 2 of the Yilgarn Gold Exploration Targeting Atlas (Report 132): Geological Survey of Western Australia, Digital data package (USB).
- Witt, WK, Ford, A, Hanrahan, B and Mamuse, A 2013, Regional-scale targeting for gold in the Yilgarn Craton: Part 1 of the Yilgarn Gold Exploration Targeting Atlas: Geological Survey of Western Australia, Report 125, 130p.

RECORD 2023/5

# SPATIAL TRENDS AND RELATIONSHIPS EMERGING FROM THE SYSTEMATIC CLASSIFICATION OF GRANITIC ROCKS OF THE YILGARN CRATON

RH Smithies, JR Lowrey, DC Champion, Y Lu and K Gessner

## Access GSWA products



### All products

All GSWA products are free to download as PDFs from the DMIRS eBookshop <[www.dmirs.wa.gov.au/ebookshop](http://www.dmirs.wa.gov.au/ebookshop)>. View other geoscience information on our website <[www.dmirs.wa.gov.au/gswa](http://www.dmirs.wa.gov.au/gswa)>.



### Hard copies

Limited products are available to purchase as hard copies from the First Floor Counter at Mineral House or via the DMIRS eBookshop <[www.dmirs.wa.gov.au/ebookshop](http://www.dmirs.wa.gov.au/ebookshop)>.



### Fieldnotes

Fieldnotes is a free digital-only quarterly newsletter which provides regular updates to the State's exploration industry and geoscientists about GSWA's latest programs, products and services. Access by subscribing to the GSWA eNewsletter <[www.dmirs.wa.gov.au/gswaenewsletter](http://www.dmirs.wa.gov.au/gswaenewsletter)> or downloading the free PDF from the DMIRS eBookshop <[www.dmirs.wa.gov.au/ebookshop](http://www.dmirs.wa.gov.au/ebookshop)>.



### GSWA eNewsletter

The GSWA eNewsletter is an online newsletter that contains information on workshops, field trips, training and other events. To keep informed, please subscribe <[www.dmirs.wa.gov.au/gswaenewsletter](http://www.dmirs.wa.gov.au/gswaenewsletter)>.



Further details of geoscience products are available from:

First Floor Counter  
Department of Mines, Industry Regulation and Safety  
100 Plain Street  
EAST PERTH WESTERN AUSTRALIA 6004  
Phone: +61 8 9222 3459 Email: [publications@dmirs.wa.gov.au](mailto:publications@dmirs.wa.gov.au)  
[www.dmirs.wa.gov.au/GSWApublications](http://www.dmirs.wa.gov.au/GSWApublications)